UNIVERSITY OF OKLAHOMA

GRADUATE COLLEGE

FLAVOR CHANGING NEUTRAL CURRENTS IN A GENERAL TWO HIGGS DOUBLET MODEL: USING AN EXTENDED HIGGS SECTOR TO SEARCH FOR NEW PHYSICS

A DISSERTATION

SUBMITTED TO THE GRADUATE FACULTY

in partial fulfillment of the requirements for the

Degree of

DOCTOR OF PHILOSOPHY

By

PHILLIP BRENTON MCCOY
Norman, Oklahoma
2017

FLAVOR CHANGING NEUTRAL CURRENTS IN A
GENERAL TWO HIGGS DOUBLET MODEL:
USING AN EXTENDED HIGGS SECTOR TO SEARCH FOR NEW PHYSICS

A DISSERTATION APPROVED FOR THE
HOMER L. DODGE DEPARTMENT OF PHYSICS AND ASTRONOMY

BY

Dr. Chung Kao, Chair

Dr. Keri Kornelson

Dr. Howard Baer

Dr. Ronald Kantowski

Dr. Ian Sellers

Acknowledgements

From the first time someone looked at the material world and asked, "I think there is something in there, something smaller, more fundamental" to the intricate and challenging work being done now with concepts and objects that cannot even be seen with the most powerful optics, the field has evolved and changed. And I am so very grateful to have been a part of that evolution.

I am also very fortunate to have been a part of this wonderful family here at OU. Their support has gone above and beyond anything anticipated or even hoped for by someone embarking on this life changing journey. I would like to especially like to thank Prof. Chung Kao, my advisor, who saw this confused but curious undergrad one summer about to enter into the crazy and sometimes stressful life of grad school and took him under his wing and helped mold him into the physicist, teacher, and person I am today.

I would also like to thank all of my committee members, Prof. Ron Kantowski, Prof. Howie Baer, Prof. Ian Sellers, Dean Keri Kornelson, and James Hawthorne for their support and interest in what I was researching. Their patience and expertise while trying to get everything finished up and frustratingly helpful leading questions to help me better understand the majesty behind some of the work I was doing. I am very fortunate to have been able to work with each and every one of them.

My experiences here and the people I met and interacted with encompass an entire experience that goes far beyond research and is something I think is unique within our department. I would like to first thank all of the physics graduate students past and present for not only their direct interactions with me but also for all they have done to make this department into the family community it is. Each one of us leaves a legacy in the form of research but also in the form of how

we shape the department, the classes we teach, and the overall community of the university.

For me, personally, I would also like to single out Baris Altunkaynak, Mike Savoy, Dylan Frizell, Hasan Serce, Hasib Ahmed, Scarlet Norberg, Othmane Rifki, Ben Pearson, David and Callie Bertsche, and Dan Mickelson. In addition to the broader physics community these individuals make up most of my core High Energy family and could always be counted on for helpful discussions of particle physics. High energy physicists are a unique bunch and there are some symmetries that get broken once you leave our local bit of phase space that don't quite translate to the other fields. I also want to sincerely think my newest brother, Rishabh Jain, for not only his helpful discussions and afternoon coffee breaks but for also being such an important, vibrant, and intelligent member of our research group. If I am to leave this work in anyone's hands I am definitely happy to leave them with you.

Outside of high energy physics is a long, long list of people who have been there for me but I would like to especially mention Shayne Cairns, Rhiannon Griffin, Jeremy Lusk, Sean Krzyzewski, Sara Barber, Tom Akin, Tim Miller, Jenna Nugent Miller, Brian Friesen, Maren Padeffke-Kirkland, and Stephane Valladier. All of you helped me get started, get through my first two years of grad school, and then countless times for countless other things during my entire time here. Together we built G-PSI and helped strengthen this department and each other and I am so glad to have worked with all of you.

As for these new young whippersnappers, I'm from Tennessee so I can use that term, who are picking up the mantle we left behind and carrying it forward on their own journey towards enlightenment, publications, and prestige. I want to thank you all for your friendship, support, and belief in me and this department. To Alex, Malia, Renae, James, Tim, Evan, Kyra, Andrew, Joseph, Soumya, Javad, Delaram, Brian, and Lisa, I wish you all the best of luck going forward both within

the department and in your future careers. I am proud to call you all friends and colleagues and look forward to where you take the department now that all of us old folks are gone. We leave it in your very capable hands.

Even before I was a grad student, or even a physicist (though that is debatable), I had the love and support of my wonderful family and friends. Their love, encouragement, and support for what I wanted to study even if they had no idea what it was made all of this possible. You all encouraged me from day one to pursue whatever made me happy, even if that was cringe worthy at times, and gave me the role models and examples I needed to succeed. My mom and grandmother were always there to lend an ear whenever I had a student to complain about, and my dad when I was fighting with my computer over some piece of code or another, my aunt and step-dad whenever I needed encouragement for where this would lead and what life looks like once you are out of school, and my brother who not only supported what I was doing but picked up the slack with the rest of the family when I was busy working. To Michelle and her family, thank you for your help and support as I was starting out and always being willing to hear about the crazy physics I was studying out here, I wouldn't have made it through those first few years without you. And to Lauren and her family who welcomed me with open arms and shared my attention with graduate school and never made me feel bad for always being busy. I look forward to being able to spend more time with you all now that I embark on this new chapter of my life.

Graduate school, as I have learned, is more than just the research. Its also about building you up as a person, helping mold and shape the way you think and what you do. I have met so many amazing people here and had so many amazing experiences that would have been impossible to have anywhere else. To the office staff at OU who helps keep all of that in motion, thank you so very much. This place really would fall apart without you. And to the faculty who help make the

department the powerhouse of research and education it is, thank you for your investments in us and the work you do every day to make it a place where we can learn and grow. You all will forever be one of our the department's and the university's greatest assets.

There are even more people to thank than I could have mentioned here. Quantum mechanics taught us long ago that our state is influenced by each and every interaction we experience, positive and negative, and I can attest to the truth of that even macroscopically. I am who I am today in no small part because of the work I did at OU and the people I met and I will always remember that.

"*The strongest bonds come from families – those we are born into and those we choose.*"
— Jeff Wheeler, *Poisonwell*
(Whispers from Mirrowen, #3)

Table of Contents

List of Tables

List of Figures

Abstract

In this dissertation I present studies of flavor-changing neutral Higgs interactions in a general Two Higgs Doublet Model. I focus on the analytic calculation of $\phi^0 \to tc$ and $\phi^0 \to \tau\mu$ where $\phi^0 = h^0,\ H^0,\ A^0$. In the case of the tc state we look at production from heavy Higgs states, H^0 and A^0, associated production with a top from charmed initial states, and associated production of a Higgs with a charm from a $t\bar{t}$ intermediate state. In the $\tau\mu$ channel we only consider $\tau\mu$ production from the light, or Standard Model-like, Higgs boson, h^0, and the heavy Higgs states. In all cases I present calculated discovery potentials for finding these rare, beyond Standard Model decays at the Large Hadron Collider for the 13 TeV and 14 TeV data sets with integrated luminosities of 30, 300, and 3000 fb^{-1}.

Chapter 1

The Standard Model

> "*If I have seen further, it is by standing on ye shoulders of giants.*"
>
> — Sir Isaac Newton, *Letter from Sir Isaac Newton to Robert Hooke*

The Standard Model (SM) of particle physics is one of the most successful and precise theories in physics to date. It contains the culmination of our knowledge involving the fundamental constituents of matter and how they interact with one another. It also provides a framework on which we can analyze experimental data and make predictions for what happens when these particles collide at ultrarelativistic speeds. Experiments to probe these limits and energy scales exist around the globe as a collaborative effort involving several countries and thousands of scientists and universities. One of the most notable of these collaborations being the *Conseil Européen pour la Recherche Nucléaire*, (CERN) [b]. Here the largest particle collider ever built, the Large Hadron Collider (LHC), is operated by researchers across the world in several collaborations such as, ATLAS, CMS, Alice, and LHCb to name but a few. It is the LHC and specifically the ATLAS and CMS collaborations that form the focus and impetus of this dissertation. Let us begin our journey with the formation and structure of the lauded SM and why it is we know there is more yet to discover about the fundamentals of nature.

[b] About CERN `http://home.cern/about`

1.1 Composition and group structure

We begin our dicussion of the SM with a look at its structure and makeup. As mentioned, the SM is not only a collection of the fundamental particles but also describes how those particles interact. To aid with our terminology it is best to start with what are the fundamental particles of nature and later I will address the interactions that are significant to this work in particular.

1.1.1 Composition

Matter, as we observe and interact with on a regular basis, is made up predominately of protons, neutrons, and electrons. Along with these main components, we observe and measure matter, in many cases, through the use of light, electromagnetic waves that interact with matter as packets or "quanta" of energy that we call photons. As it turns out, electrons and photons are the first of our fundamental particles. Protons and neutrons, however, have an underlying structure that containing particles classified as fermions and bosons.

Fermions

Fermions are particles that have $1/2$ integer spin, with the exception of neutrinos, carry electric charge. They are further subdivided into two categories called leptons and quarks. The electron, e, that we mentioned before is the first lepton in our picture of nature and has two other compatriots known as the muon, μ, and tau, τ. Each of these leptons has integer charge $\pm e$ and has a corresponding neutral partner called the neutrino: $\nu_e,\ \nu_\mu,\ \nu_\tau$, that have almost no measureable mass. Without much mass and with no electric charge they interact with only a limited number of other particles, which makes them especially difficult to detect. Each pair of lepton and corresponding neutrino form generations and are often organized

in doublets,

$$\begin{pmatrix} \nu_e \\ e \end{pmatrix}, \quad \begin{pmatrix} \nu_\mu \\ \mu \end{pmatrix}, \quad \begin{pmatrix} \nu_\tau \\ \tau \end{pmatrix} . \tag{1.1}$$

Quarks are the other fermionic particles in the SM and are likewise split up into three generations and organized into doublets, Equation (**1.2**). Unlike the leptons, quarks have fractional charge and also have a quantum number known as color charge. The 'up-type' quarks: up, charm, and top, have a charge of $^{2}/_{3}e$ and the 'down-type' quarks; down, strange, and bottom; have a charge of $^{-1}/_{3}e$. Of these six quarks, it is the up and down quarks that contribute the most to the behavior of the protons and neutrons and are referred to as 'valence' quarks. Specifically, the proton has two up quarks and one down quark as its valence quarks and the neutron has one up quark and two down quarks as its valence quarks. The term valence in this respect simply means that of the quarks one might find in a proton or neutron the valence quarks contain the largest fraction of the proton's or neutron's energy. The distribution of the quarks and gluons as functions of the energy fraction they carry from the parent proton or neutron is called, the parton distribution function (PDF) [1, 2].

$$\begin{pmatrix} u \\ d \end{pmatrix}, \quad \begin{pmatrix} c \\ s \end{pmatrix}, \quad \begin{pmatrix} t \\ b \end{pmatrix} . \tag{1.2}$$

Bosons

In addition to fermions, which follow Fermi-Dirac statistics and have half-integer spin we also have particles with integer spin that follow Bose-Einstein statistics and are thus called bosons. Their ranks include the gluons, W and Z bosons, the photon, and the Higgs boson. All except for the Higgs are considered

gauge bosons and mediate one of the fundamental forces of nature: the strong force, the weak force, and the electromagnetic force.

The W and Z bosons; W^+, W^-, Z; mediate the weak force and interact with any particle that has weak hypercharge and are observed mostly in neutrino scattering and nuclear interactions such as interchange between protons an neutrons. The gluons, g_a^μ, mediate the strong force and interact with any particle that has color charge. In the SM this means that quarks are the only particles that couple directly to the gluons. The strong force is predominately realized as the force that holds the nucleons together by binding the quarks in the nucleons, protons and neutrons, together. This leads to a phenomenon known as quark confinement where at low energies we do not see any quarks that are not bound inside of some composite object. The last gauge boson that exists in the SM is the photon, γ, which mediates the well known electromagnetic force and interacts directly with any particles that have electric charge. Gravity remains the only fundamental force that the SM does not incorporate.

1.1.2 Group structure

The particles that make up the SM are resonances of fields that are described within a set of mathematics known as group theory. Each group contains information about the particle fields and information on how particle states are created, destroyed, and evolve in space and time. In the SM the group structure is $SU(3)_c \otimes SU(2)_L \otimes U(1)_Y$. The order of each group can tell us how many unique generators, and thus bosons, the group contains. For example, $SU(3)_c$ is third order and so contains $3^2 - 1 = 8$ unique generators giving us eight gluons, G_a^μ. Following that example, $SU(2)_L$ has three unique generators giving us the three W bosons, W_1^μ, W_2^μ, and W_3^μ. This leaves $U(1)_Y$ which has only one generator

that gives rise to the B^μ boson. When we bring these fields together with the other elementary particles we can construct the SM Lagrangian density in its most concise form:

$$\begin{aligned}\mathcal{L} = &-\frac{1}{4}\left[B^{\mu\nu}B_{\mu\nu} + W^{i\mu\nu}\cdot W_{i\mu\nu} + G_a^{\mu\nu}G_{a\mu\nu}\right] \\ &+ \overline{\psi}\left(i\gamma^\mu D_\mu - m\right)\psi + \overline{\psi}_j\left(i\gamma_\mu D'^{\mu}_{jk} - M_j\delta_{jk}\right)\psi_k \\ &+ \left(D^\mu\Phi\right)^\dagger\left(D_\mu\Phi\right) - \sum_f \lambda_f\left(\overline{\psi}_L\Phi\psi_R + \overline{\psi}_R\widetilde{\Phi}\psi_L\right) - V(\Phi)\,, \\ i = 1,2,3 \qquad &\text{and} \qquad a = 1,2,\ldots,8. \end{aligned} \tag{1.3}$$

We can expand this further with the following definitions:

$$D_\mu = \partial_\mu + ig'\frac{Y}{2}B_\mu + igt^iW_\mu^i\,, \tag{1.4}$$

$$D'^{\mu}_{jk} = \delta_{jk}\partial^\mu + ig_3(T_a)_{jk}G_a^\mu\,, \tag{1.5}$$

$$\overline{\psi}\psi = \overline{\psi}_L\psi_R + \overline{\psi}_R\psi_L\,, \tag{1.6}$$

where

$$\psi_{L,R} = \frac{1}{2}(1 \mp \gamma_5)\ . \tag{1.7}$$

In the above definitions, we also need to take special care with the scalar field, Φ, which is the Higgs field. It is important to distinguish that,

$$\Phi = \begin{pmatrix}\phi^+ \\ \phi^0\end{pmatrix} \quad \text{and} \quad \widetilde{\Phi} = S\Phi = \begin{pmatrix}\phi^{0^*} \\ -\phi^-\end{pmatrix}\,, \tag{1.8}$$

where

$$S = i\sigma_2 = \begin{pmatrix}0 & +1 \\ -1 & 0\end{pmatrix}\ . \tag{1.9}$$

All of the rank two tensors above represent the gauge boson field strength, the ψ terms represent the fermion fields, the γ_μ term is the Dirac matrices associated with the fermions, the m and M terms represent mass matrices for the fermions, and Φ is the Higgs field. The coupling between the fermions and Higgs fields is referred to as the Yukawa portion of the Lagrangian. Here the λ_f terms show the couplings between the Higgs field and the fermions. For leptons λ_f define the entire coupling, for the quarks, however, they include an additional color tensor, G^{ab}, F^{ab}:

$$\text{up-type quarks: } \lambda_u \equiv F^{ab}\,, \tag{1.10}$$

$$\text{down-type quarks: } \lambda_d \equiv G^{ab}\,. \tag{1.11}$$

As mentioned before, the total group structure of the SM is $SU(3)_c \otimes SU(2)_L \otimes U(1)_Y$, where D_μ, Equation (**1.4**), is the electroweak covariant derivative and D'^{μ}_{jk}, Equation (**1.5**). Together these two terms handle all couplings between the gauge bosons and the other fields of the SM. If you look once more at Equation (**1.3**), you will notice that the Higgs field is only operated on by the electroweak covariant derivative and is not part of the $SU(3)_c$ group structure despite the presence of color matrices in the Yukawa terms. This situation brings about some interesting possibilities, namely in regard to the Higgs Mechanism and the breaking of the electroweak symmetry.

When we combine $SU(2)_L$ with $U(1)_Y$ we get $SU(2)_L \otimes U(1)_Y$ which is the group structure of electroweak theory. When the electroweak symmetry is broken, the W_1^μ and W_2^μ to mix and W_3^μ and B^μ mix to generate the physical bosons,

$W^{\pm}$, Z and A (photon), Equation (**1.12**a),

$$\begin{pmatrix} Z^{\mu} \\ A^{\mu} \end{pmatrix} = \begin{pmatrix} \cos\theta_W & -\sin\theta_W \\ \sin\theta_W & \cos\theta_W \end{pmatrix} \begin{pmatrix} W_3^{\mu} \\ B^{\mu} \end{pmatrix} \ , \tag{**1.12**a}$$

$$\begin{pmatrix} W^{+} \\ W^{-} \end{pmatrix} = \frac{1}{\sqrt{2}} \begin{pmatrix} 1 & -i \\ i & 1 \end{pmatrix} \begin{pmatrix} W_1^{\mu} \\ W_2^{\mu} \end{pmatrix} \ . \tag{**1.12**b}$$

This formulation can technically exist independent of the electroweak symmetry breaking (EWSB) but is not particularly motivated by anything physical. When EWSB occurs spontaneously, however, the W and Z bosons can acquire a mass while the photon, A^{μ}, remains massless. The breakdown and mixing of the fields then has meaning as the bosons are now distinguishable from one another.

1.2 The Higgs mechanism

The Higgs mechanism is a process by which the $SU(2)_L \otimes U(1)_Y$ symmetry is broken by the vacuum expectation value of the Higgs Field, and by which particles acquire mass without having to break the overall symmetry of the Lagrangian. When the electroweak, $SU(2)_L \otimes U(1)_Y$, symmetry is broken the Higgs potential acquires a vacuum expectation value (VEV) that is unique and causes the couplings between the fundamental particles and the Higgs boson to be proportional to the particle's mass. This effect is a consequence of minimizing the Higgs potential,

$$V(\Phi) = \mu^2 \Phi^{\dagger}\Phi + \lambda \left(\Phi^{\dagger}\Phi\right)^2 \ . \tag{**1.13**}$$

When the above potential is minimized according to standard calculus techniques we have:

$$\frac{\partial V(\Phi)}{\partial|\Phi|} = 2\mu^2|\Phi| + 4\lambda|\Phi|^3 = 0 \tag{1.14}$$

which produces two options for the minimum value of Φ

$$|\Phi| = \pm\left(\frac{-\mu^2}{2\lambda}\right)^{1/2} . \tag{1.15}$$

At this point we seemingly have 'two' choices for the minimum of the Higgs potential, call them $\pm V_0$. Without losing generality, we can shift the potential with a constant as expected but it does nothing to offset the minima as shown in Figure **1.1**. However, if the Higgs field were to make a choice, say choose $+V_0$ or $-V_0$, then the minimum would take on a defined value and now $\langle 0|\Phi|0\rangle \neq 0$ but takes on an expectation value, called v or the VEV. Generally, a break in a symmetry for a particular field would disrupt the overall symmetry of the Lagrangian but in the case of scalar particles that is not true. More specifically, $\mathcal{L}(\Phi) = \mathcal{L}(-\Phi)$ but $V(V_0) \neq V(-V_0)$.

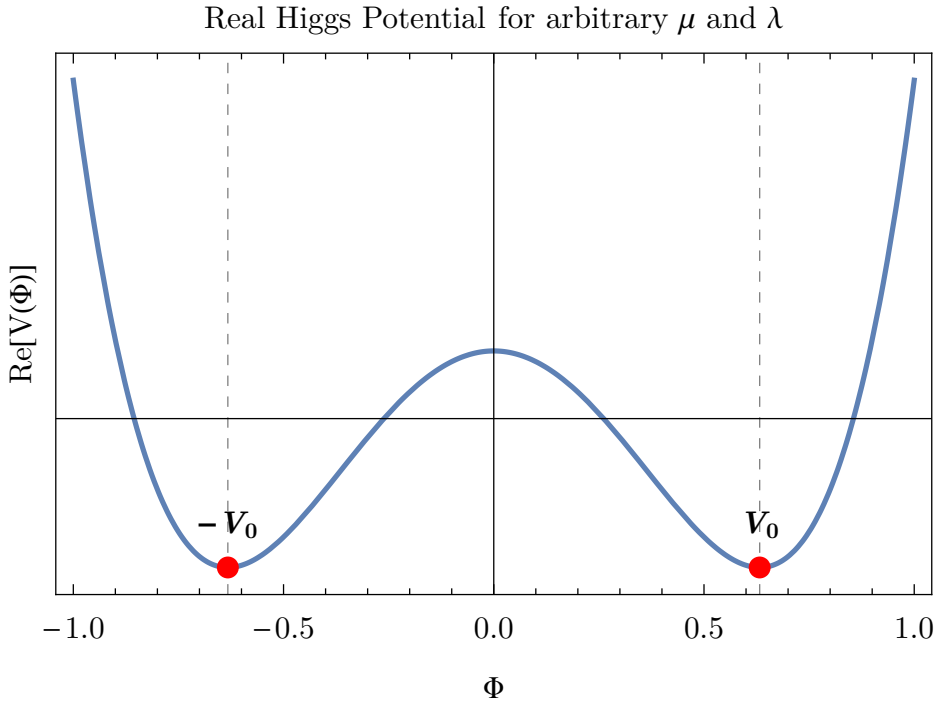

Figure 1.1: This is a graphical representation of the real part of the complex Higgs potential, Equation (**1.13**), also known as the 'Mexican Hat Potential'. $\pm V_0$ indicate the values of the Higgs minimum possible. When electroweak symmetry is broken, the Higgs field preferentially chooses the $+V_0$ minimum.

This is a simplistic picture but instructive in how well it represents the dichotomy of the minimum of the Higgs potential. Realistically, since this is based on a complex field, this is a bit more complicated. What is depicted above, then, is the real part of the Higgs potential. Figure **1.2** shows a truer picture of how the minimum looks and looks slightly more emblematic of the moniker " mexican Hat potential," but the results describe are fundamentally no different, if not a bit more striking now. Instead of two choices of minimum value, there are an infinite number of choices creating a circle in the complex plane, however, we often choose a real, positive minimum, $+V_0$ from Figure **1.1**, instead of a real, negative or complex value.

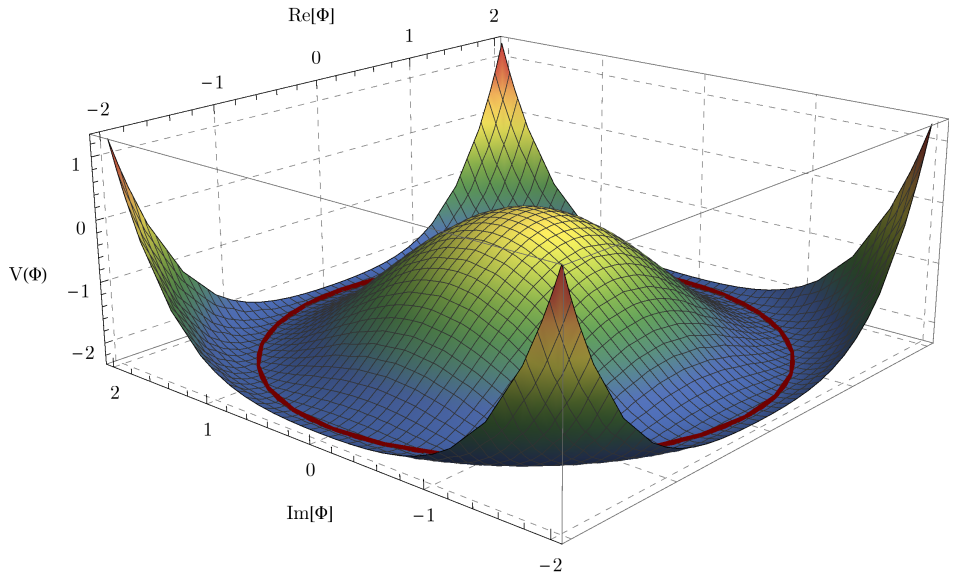

Figure 1.2: This is a graphical representation of the complex Higgs potential, Equation (**1.13**), potential. The dark ring in the crease denotes the possible values that minimize the Higgs potential. The $\pm V_0$ shown in Figure **1.1**, occur as $\mathrm{Im}\,(\Phi) \to 0$.

Once the Higgs field obtains a VEV, its effects on the rest of the particles in the Lagrangian start to become apparent. We can now represent Φ more completely:

$$\Phi = \frac{1}{\sqrt{2}} \begin{pmatrix} \sqrt{2}G^{+} \\ \phi^{0} + iG^{0} \end{pmatrix}, \tag{1.16a}$$

where

$$\phi^{0} = \frac{1}{\sqrt{2}}(H + v)\,. \tag{1.16b}$$

Here, H or h^0 as it is also referred to, is the physical Higgs boson, the discovery of which was announced on July 4, 2012, [3, 4]. After the Higgs VEV is obtained, the W, Z, and fermions all become massive while preserving the symmetry of the Lagrangian. The G terms in the Higgs field above are Goldstone bosons. They are consumed by the electroweak gauge fields and give them mass. In the leptonic

sector we must work with a new representation of the Yukawa terms,

$$\mathcal{L}_Y = -\lambda_e \, \overline{E}_L \Phi \, e_R - \lambda_e \, \overline{e}_R \Phi^\dagger \, E_L - F^{ab} \, \overline{Q}^a_L \Phi \, d^b_R - G^{ab} \, \overline{Q}^a_L \, \widetilde{\Phi} \, u^b_R \,, \qquad (\mathbf{1.17})$$

where $\psi_{L,R}$ have been changed to E_L, e_R, Q_L, and $(d/u)_R$ to denotes the left-handed lepton doublet, right handed lepton singlet, left-handed quark doublet, and the right-handed quark singlets respectively. The doublet fields are of the form,

$$E_L = \begin{pmatrix} \nu_\ell \\ e_\ell \end{pmatrix} \,, \qquad (\mathbf{1.18}\text{a})$$

$$Q_L = \begin{pmatrix} u_L \\ d_L \end{pmatrix} \,, \qquad (\mathbf{1.18}\text{b})$$

with $e_{L,R}$ and $(u/d)_{L,R}$ are generic lepton and quark fields that need to be summed over. When we apply the form of the Higgs field from Equation (**1.16**b), we find that not only do the neutrino fields not interact with the Higgs but we only get pairs of u_L, u_R and d_L, d_R that survive. All cross terms vanish and we are left with

$$\begin{aligned} \mathcal{L}_Y = &-\lambda_e \, \overline{e}_L^{-} \left(\frac{H+v}{\sqrt{2}} \right) e_R - \lambda_e \, \overline{e}_R^{-} \left(\frac{H+v}{\sqrt{2}} \right) e_L^{-} \\ &- F^{ab} \, \overline{d}_L^{\,a} \left(\frac{H+v}{\sqrt{2}} \right) d_R^{\,b} - G^{ab} \, \overline{u}_L^{\,a} \left(\frac{H+v}{\sqrt{2}} \right) u^b_R \,. \end{aligned} \qquad (\mathbf{1.19})$$

The terms that couple to the VEV then form the mass terms for the fermions,

$$-\mathcal{L}_Y = \overline{e}_L{}^- \ \widetilde{M}_\ell \ e_R + \overline{d}_L{}^a \ \widetilde{M}_d^{ab} \ d_R^b + \overline{u}_L{}^a \widetilde{M}_u^{ab} \ u_R^b \,, \tag{1.20}$$

where

$$\widetilde{M}_\ell = \frac{\lambda_e v}{\sqrt{2}} \qquad \widetilde{M}_d^{ab} \ = \frac{v}{\sqrt{2}} F^{ab} \qquad \widetilde{M}_u^{ab} = \frac{v}{\sqrt{2}} G^{ab} \,. \tag{1.21}$$

All that remains then is to diagonalize the mass matrices by applying bi-unitary transformations to the lepton and quark fields,

$$e'_L = L_L \ e_L \qquad u'_L{}^a = U_L^{na} \ u_L{}^a \qquad d'_L{}^b = D_L^{mb} \ d_L{}^b \,, \tag{1.22}$$

and

$$e'_R = L_R \ e_R \qquad u'_R{}^a = U_R^{na} \ u_R^a \qquad d'_R{}^b = D_R^{mb} \ d_R{}^b \,. \tag{1.23}$$

When we diagonalize the mass matrices and sum over $\ell, /a, /b, /m,$ and n the eigenvalues fall out naturally and the matrices take on an easily decipherable form,

$$L_L^\dagger \ \widetilde{M}_\ell \ L_R = M_{\rm L} = \begin{pmatrix} m_e & 0 & 0 \\ 0 & m_\mu & 0 \\ 0 & 0 & m_\tau \end{pmatrix} , \tag{1.24}$$

$$U_L^{\dagger \ an} \ \widetilde{M}_u^{nm} \ U_R^{ma} = M_U = \begin{pmatrix} m_u & 0 & 0 \\ 0 & m_c & 0 \\ 0 & 0 & m_t \end{pmatrix} , \tag{1.25}$$

$$D_L^{\dagger \ bn} \ \widetilde{M}_d^{nm} \ D_R^{mb} = M_D = \begin{pmatrix} m_d & 0 & 0 \\ 0 & m_s & 0 \\ 0 & 0 & m_b \end{pmatrix} . \tag{1.26}$$

Feeding these results back into the Yukawa coupling we can finally see the effect of the Higgs VEV on the fermion fields and how the particles 'acquire' mass. A more correct statement would be that the strength of the coupling between the particle and the Higgs field is proportional to the particle's mass but it is in some senses a 'chicken or the egg' situation due to how closely they are tied together,

$$m_\ell = \frac{v}{\sqrt{2}}\,\lambda_\ell \quad \text{where} \qquad \ell = e,\ \mu,\ \tau\ ; \tag{1.27}$$

$$m_a = \frac{v}{\sqrt{2}}\,\lambda_{aa} \quad \text{where} \qquad a = u,\ c,\ t\ ; \tag{1.28}$$

$$m_b = \frac{v}{\sqrt{2}}\,\lambda_{bb} \quad \text{where} \qquad b = d,\ s,\ b\ . \tag{1.29}$$

We can then define the Yukawa couplings in terms of the particle mass and see directly how strongly the Higgs field couples to each particle, $\lambda_\ell = \sqrt{2}\,\dfrac{m_\ell}{v}$, $\lambda_{aa} = \sqrt{2}\,\dfrac{m_a}{v}$, and $\lambda_{bb} = \sqrt{2}\,\dfrac{m_a}{v}$. This rounds out the SM and how the picture of interactions starts to come together but there are still several unanswered questions that leads us to believe there is more than meets the eye, so to speak.

1.3 Need for new physics

The SM is the most well tested and precise theory to date with the original formulation of Quantum Electrodynamics (QED) in 1948 [5–8], to the development of gauge theories in 1954 [9], the prediction and later discovery of CP-violation [10], the introduction of Quantum Chromodynamics (QCD) in 1973 [11], and culminating with the discovery of the Higgs boson in 2012 at the LHC. Despite all of its success, however, the SM does have some limitations. In some ways it is similar to Newtonian mechanics, in the range of its validity and for select topics, the SM expertly explains and predicts the physics of fundamental particle

interactions. Just like Newtonian mechanics and relativity, at some point, nature calls for a different approach to particle interactions that can offer a more complete picture of what is going on.

For instance, If we include gravity in the SM, we generate large divergences at high energy scales [12]. While we have observational evidence of dark matter, no candidate for such a particle exists in the SM [13]. As mentioned previously, neutrinos do not appear in the Yukawa term of the Lagrangian but are observed to have non-zero mass; but there is no mechanism for this in the SM [14]. Cosmologists and astrophysicists have continually verified that there is a large asymmetry between matter and anti-matter in our observable universe but there is no explanation for this in the SM [15]. Furthermore, though we have discovered a SM-like Higgs boson matching the predicted mass of 125 GeV, we do not well understand how the nearly infinite corrections to the Higgs mass term are cancelled [16].

To address these concerns, theorists have proposed several extensions to, and replacements for, the SM but so far none have been observed experimentally. Some of the most notable of these theories are supersymmetry (SUSY) [17], multi-verse theories [18], and string theories [19, 20]. Inside each of these broader areas of study are several select models that contain different features or focus on answering specific questions left open by the SM. In addition to full theoretical frameworks that have been developed there are also highly focused areas where certain sectors are emphasized and the implications of extending those sectors are worked out. In the dark matter realm, for instance, the QCD sector is addressed where Peccei and Quinn introduced a new particle known as the axion and a subsequent symmetry to explain the lack of observed CP-violation in the gluon sector [21]. In a similar fashion, much work has been done in extending the Higgs sector in what are called Multi-Higgs Doublet Models (MHDMs) [10]. One of the most common of which is a Two-Higgs Doublet Model (2HDM), [22].

1.4 The Two Higgs Doublet Model (2HDM)

The extended Higgs sector models are of particular interest as they are also required by all SUSY theories and can have implications for other searches being conducted. As the Higgs boson is the most recently discovered particle, the sector in which the Higgs field operates is one of the least experimentally constrained areas in modern day particle physics. This is partly because of the high mass of the SM Higgs boson but also because of the large QCD background associated with the dominant decay modes of the Higgs [23]. In fact, the original discovery channels were in the ZZ and $\gamma\gamma$ channels which collectively only make up about 2.6% of the total decay width of the SM Higgs, meaning $\approx 98\%$ of the time the Higgs will decay into something other than these two states. For these reasons it was a logical place for a pioneering young graduate student to start their search for evidence of new physics. Before we get to that, however, let us take a closer look at how one goes about adding an additional doublet to an area of particle physics.

In the SM, there is a single Higgs field, Φ, which has the doublet representation shown in Equation (**1.16**a). In a 2HDM we append this with an additional doublet of a similar form, so in place of one scalar Higgs field we now have two, Φ_1 and Φ_2 [24],

$$\Phi_a = \begin{pmatrix} \phi_a^+ \\ (v_a + \rho_a + i\eta_a)/\sqrt{2} \end{pmatrix}, \quad a = 1,\, 2\ , \tag{**1.30**}$$

where ϕ, ρ, and η are all boson fields. Technically, since the Higgs potential is now dependent on two fields, each field can have its own VEV when the potential is

minimized, [25],

$$\begin{aligned} V = {} & m_{11}^2 \Phi_1^\dagger \Phi_1 + m_{22}^2 \Phi_2^\dagger \Phi_2 - \left[m_{12}^2 \Phi_1^\dagger \Phi_2 + \text{H.c.} \right] \\ & + \frac{1}{2}\lambda_1 (\Phi_1^\dagger \Phi_1)^2 \frac{1}{2}\lambda_2 (\Phi_2^\dagger \Phi_2)^2 + \lambda_3 (\Phi_1^\dagger \Phi_1)(\Phi_2^\dagger \Phi_2) + \lambda_4 (\Phi_1^\dagger \Phi_2)(\Phi_2^\dagger \Phi_1) \\ & + \left\{ \frac{1}{2}\lambda_5 (\Phi_1^\dagger \Phi_2)^2 + \left[\lambda_6 (\Phi_1^\dagger \Phi_1) + \lambda_7 (\Phi_2^\dagger \Phi_2) \right] \Phi_1^\dagger \Phi_2 + \text{H.c.} \right\} . \end{aligned} \tag{1.31}$$

However, the two VEV's are not unrelated and we can apply a rotation angle that allows us to talk about one vacuum expectation value in terms of another following the form

$$\begin{pmatrix} v_1 \\ v_2 \end{pmatrix} = \begin{pmatrix} \cos\beta & -\sin\beta \\ \sin\beta & \cos\beta \end{pmatrix} \begin{pmatrix} v \\ 0 \end{pmatrix} , \tag{1.32}$$

which results in:

$$v_1 = v\cos(\beta) \qquad v_2 = v\sin(\beta) \qquad \frac{v_2}{v_1} = \tan(\beta) . \tag{1.33}$$

This transformation is then applied to the remaining fields and allows us to the represent the two Higgs doublets in a more familiar form

$$\Phi_1 = \frac{1}{\sqrt{2}} \begin{pmatrix} \sqrt{2}\left(G^+ \cos\beta - H^+ \sin\beta\right) \\ v\cos\beta + H_1 + i\left(G^0 \cos\beta - A^0 \sin\beta\right) \end{pmatrix} , \tag{1.34a}$$

$$\Phi_2 = \frac{1}{\sqrt{2}} \begin{pmatrix} \sqrt{2}\left(G^+ \sin\beta + H^+ \cos\beta\right) \\ v\sin\beta + H_2 + i\left(G^0 \sin\beta - A^0 \cos\beta\right) \end{pmatrix} , \tag{1.34b}$$

where G^+ and G^0 are Goldstone bosons that get absorbed by the W and Z fields as they did in the SM to gain mass. This leaves us now with four unique Higgs fields: $H_{1,2}$, A^0, H^+, and one conjugate field, H^-, [26].

Separately, the two neutral scalar states, H_1 and H_2, can be represented in the

physical basis through a similar transformation through another rotation angle, α, called the Higgs mixing angle,

$$\begin{pmatrix} H_1 \\ H_2 \end{pmatrix} = \begin{pmatrix} \cos\alpha & -\sin\alpha \\ \sin\alpha & \cos\alpha \end{pmatrix} \begin{pmatrix} H^0 \\ h^0 \end{pmatrix} . \tag{1.35}$$

To see how this impacts the physics of interactions it is helpful to look at the mass terms in the Yukawa Lagrangian for this new model,

$$\begin{aligned} \mathcal{L}_Y = &- \rho_1^{\ell} \overline{E}_L \Phi_1 \; e_R - \rho_2^{\ell} \overline{E}_L \Phi_2 \; e_R - \rho_1^{D} \; \overline{Q}_L \Phi_1 \; d_R - \rho_2^{U} \; \overline{Q}_L \Phi_2 \; d_R \\ &- \rho_1^{U} \; \overline{Q}_L \; \widetilde{\Phi}_1 \; u_R - \rho_2^{U} \; \overline{Q}_L \; \widetilde{\Phi}_2 \; u_R \, , \end{aligned} \tag{1.36}$$

where $\rho^{U,D,\ell}$ represent the up-type quark, down-type quark, and lepton coupling matrices respectively. The new fermion masses take on a new form,

$$M^F = \frac{v}{\sqrt{2}} \left(\rho_1^F \cos\beta + \rho_2^F \sin\beta \right) , \tag{1.37}$$

where $F = \{U, D, \ell\}$. We can then define a new coupling matrix, κ^F, based on comparing the above mass terms with those in Equations (**1.27**) to (**1.29**),

$$\kappa^F \equiv \rho_1^F \cos\beta + \rho_2^F \sin\beta \, . \tag{1.38}$$

In addition to this new coupling matrix, κ^F, we also end up creating an orthogonal coupling matrix, ρ^F, that does not participate in the mass interactions

$$\rho^F \equiv -\rho_1^F \sin\beta + \rho_2^F \cos\beta \, . \tag{1.39}$$

Leading to a new Yukawa Lagrangian,

$$\begin{aligned}\mathcal{L}_Y = &-\frac{1}{\sqrt{2}}\sum_{F=U,D,L}\overline{F}\left[\left(\kappa^F s_{\beta-\alpha}+\rho^F c_{\beta-\alpha}\right)h^0+\left(\kappa^F c_{\beta-\alpha}-\rho^F s_{\beta-\alpha}\right)H^0\right]F\\&+\frac{1}{\sqrt{2}}\sum_{F=U,D,L}\overline{F}\left[i\,\mathrm{sgn}(Q_F)\rho^F A^0\right]P_R F\\&-\overline{U}\left(V\rho^D P_R-\rho^{U\dagger}V P_L\right)DH^+-\overline{\nu}\left(\rho^L P_R\right)LH^+ + \text{H.c.}\,, \qquad (\mathbf{1.40})\end{aligned}$$

where $c_{\beta-\alpha}\equiv\cos(\beta-\alpha)$, $s_{\beta-\alpha}\equiv\sin(\beta-\alpha)$, and $P_{L,R}=(1\mp\gamma_5)/2$.

1.4.1 Flavor changing neutral currents

In the Lagrangian above, Equation (**1.40**), we take note that although the ρ^F terms do not participate in the mass interactions of the fermions they do still partially govern the coupling of fermions to our Higgs fields. Of particular interest are the couplings involving these ρ^F matrices and the neutral Higgs fields: the light Higgs, h^0, the heavy Higgs, H^0, and the pseudoscalar Higgs, A^0. Since the ρ^F matrices do not participate in the mass terms they can have off diagonal elements that survive the diagonalization of the mass matrices. It is these off-diagonal terms that produce the phenomenon known as flavor changing currents and since they happen in relation to the neutral Higgs field they are flavor changing neutral current (FCNC) processes. These are of particular interest as they are not possible at the *tree-level*, or leading order level, in the SM and are further suppressed in higher orders by the GIM mechanism involving cancellations between diagrams involving up and charm quarks [27].

In many supersymmetric theories FCNCs are suppressed by imposing a symmetry on the Higgs sector where the two Higgs doublets couple preferentially to either up-type quarks or down-type quarks but not both [26]. In those theories

the suppression due to an additional symmetry is desired so that the lack of such signatures in the SM can be better explained within the SUSY framework. In general, however, this is not necessary as they can be controlled through the mixing angles, β and α, instead. We call the limit where the 2HDM exactly reproduces the SM, not unlike the low energy limit of relativity, the alignment limit and is benchmarked by $\sin(\beta - \alpha) \to 1$. This effectively destroys any tree-level FCNC process involving the light, or SM-like, Higgs field h^0, while also removing any effects the heavy Higgs field may have on fermion masses. Current data favors the alignment limit [28, 29] meaning a heavy Higgs FCNC process is favorable but there has been some evidence to suggest that FCNC processes may be present in the leptonic sector [30]. These processes are the focus of this dissertation and the beginning of our journey starts with how a Higgs boson with a mass of at least 125 GeV is produced in the energetic collision of two protons deep underground in an area in northern France and southern Switzerland.

Chapter 2

Analytic Higgs Production

"*Tiny, but fierce.*"
— Sanya, *Changes, Jim Butcher*

2.1 Higgs production modes

Higgs production at the LHC is generated predominately through either quark anti-quark annihilation or gluon gluon fusion. Of course, the Higgs can couple to any particle that has mass but any other modes will generate additional particles that may be detected if they are of a high enough energy.

2.1.1 Dominant processes

The dominant processes used in our study of FCNH processes involved gluon gluon fusion through a heavy quark loop, such as a top or bottom. Despite the gluon fusion production being a higher order process, the abundance of gluons in the proton help to enhance its Higgs production rate, Figures **2.1**(a) and **2.1**(b), over the tree level $q\bar{q}$ process, Figure **2.2**(c).

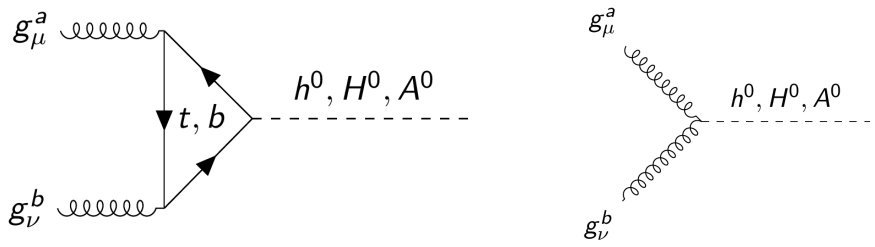

(a) Feynman diagram for the gluon-gluon fusion production mode for the Higgs boson.

(b) Feynman diagram for the effective gluon-gluon fusion production mode for the Higgs boson.

Figure 2.1: Feynman diagrams for the gluon-gluon fusion process showing the loop-level and tree-level diagrams where time is moving from left to right in the figures. Here the top and bottom contributions are listed as the couple most strongly to the Higgs and will be your dominant loop particles.

2.1.2 Sub-dominant processes

The sub-dominant processes are generally disregarded in our calculations as they introduce additional final state particles that we can exclude with careful selection criteria. However, they are worth introducing as they help illustrate the coupling behavior of this Higgs and why we must treat it so carefully. All of the diagrams are t-channel diagrams where the Higgs is produced in association with some number of jets, again, if we require, in our selection criteria, only jets associated with the immediate Higgs decay we are interested in be present in our final state we can effectively remove these additional contributions. They could be included later if we wanted additional channels in which to study Higgs production and decay but will introduce additional background processes that may be difficult to reduce without ignoring too many signal events. Of these additional decays, the most promising would be the $q\bar{q} \to H + jj$ decay mode as up quarks carry the dominant fraction of the proton's initial momentum after gluons. Here we signify

two light quarks that are produced in association with the Higgs as jets, j.

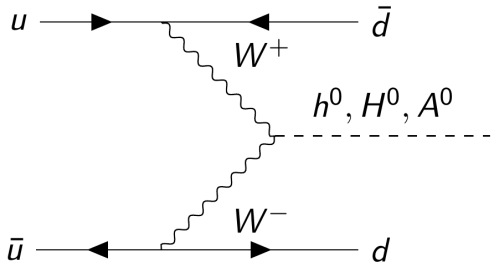

(a) Feynman diagram for the t-channel production of the Higgs from a quark and anti-quark colliding.

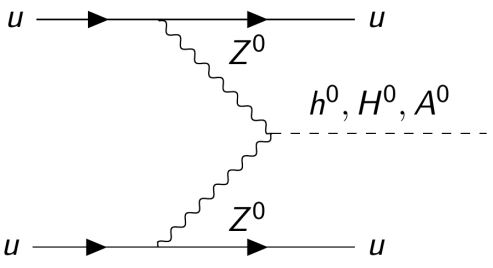

(b) Feynman diagram for the t-channel production of the Higgs from two quarks colliding.

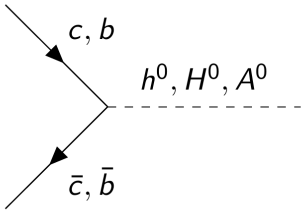

(c) Feynman diagram for the s-channel production of the Higgs from a $c\bar{c}$ or a $b\bar{b}$ in the initial colliding protons

Figure 2.2: Feynman diagrams for the sub-dominant quark quark and quark anti-quark Higgs production modes. As before, time is moving to the right in the figures. For the charm/bottom production modes we require the 5-flavor scheme for the initial colliding protons.

2.2 Effective theories

Effective theories are a broad classification of techniques used to approximate more complicated calculations or corrections. In the context of high energy physics, effective theories most commonly refer to incorporating higher order corrections into simple factors or, as is the case with this work, in reducing Loop-level calculations

to an approximate tree-level calculation. The transition can be seen in Figure **2.1**, where Figure **2.1**(a) shows the actual physical production process involving the virtual fermion loop and Figure **2.1**(b) shows the diagram for the effective theory where we have condensed the loop into an approximate tree-level coupling.

2.2.1 Loop diagrams

Loop diagrams are present in many areas of particle physics as they allow for couplings between particles that do not normally share any quantum numbers, and thus violate one or many conservation laws, and account for corrections to physical processes due to the perturbative nature of the theory. A loop is any process that is entirely virtual where the particles inside the loop are not required to be on the mass shell. Furthermore, loops are processes that happen *instantaneously* in the context of the decay process. What this means in the context of performing calculations, since $\Delta E \Delta t \geq \bar{h}/2$ by quantum mechanics, if our time is taken to be precisely known for the loop then we have no constraints on our energy.

Generally, loop diagrams are suppressed due to the presence of additional vertices and couplings associated with those vertices, and the inclusion of the propagators associated with each virtual particle. That suppression is outweighed in the case of Higgs production by a couple of factors. Gluons, for instance, carry a significant fraction of the proton's momentum, more so than even the up quarks. In addition to that, the bottom quark couples nearly four times as strongly as the next heaviest particle and the top quark nearly forty times as strongly as the bottom. These two factors combined allow the gluon-gluon fusion process to dominate Higgs production at hadronic colliders, such as the LHC.

Virtual particles

Virtual is a classification that refers to a particle or particle-like interaction that does not happen in resonance with the mass shell of the particle. In the context of the diagrams above, this is only seen in the fermion loop in the gluon gluon fusion process. Internally, to construct the transition matrix element from a virtual particle you have to apply the completeness relation from quantum mechanics and integrate over the virtual particle's momentum, which is unconstrained. Externally, when unstable particles, like the top and Higgs, are in the final state their decay products exhibit a well defined Breit-Wigner resonance at the mass value of the parent allowing us to identify them. The decay products of virtual particles in the final state, however, will produce an invariant mass peak not on the mass shell and we may need to look at additional metrics to get a clear picture of the interaction. A good example of this is in the $H \to ZZ^* \to 4\ell$ or beta decay of a neutron into a proton. The mass difference between a neutron and a proton is ≈ 1.3 MeV while the W boson that mediates this decay has a mass of ≈ 80 GeV. The neutron-proton interaction simply does not have enough energy to produce a real W boson, however, the decay process itself must be mediated by the electroweak interaction. So the W produced that subsequently generates an electron and electron antineutrino is actually a virtual W, meaning it does not exist at the mass shell. Mathematically this can be described by the equation $p^2 \neq M_W^2$, where p is the four momentum of the W [31].

Propagators and energy limits

Part of the challenge with virtual particles, especially in the context of a loop as in the gluon fusion process, is evaluating the propagators with unknown limits.

For a fermion the propagators is of the form,

$$\Delta(p) = \frac{i}{\not{p} - m + i\epsilon}$$

$$= \frac{i(\not{p} + m)}{p^2 - m^2 + i\epsilon}. \quad (\mathbf{2.1})$$

With the uncertainty in the energy because of the instantaneous nature of the loop we can have either very small or very large momenta in the denominator here. Further complications arise when we have multiple of these terms appearing due to our loop having three virtual fermion lines, each with their own propagator. Even though these particles are virtual and their lifespan is nearly instantaneous we still need the information about propagation in these terms to correctly evaluate the physical decay. In low transverse momentum situations (low P_T, we can approximate this behavior but not in high P_T cases like heavy Higgs production. So to evaluate this process as correctly as possible we need to generate an analytic solution, an analytic method for evaluating these loop processes [32].

2.3 Analytic solutions: a 'simple' alternative

The technical aspects of calculating analytic cross sections lie in the calculation of the Transition Matrix Element, often referred to as M that has to be squared in order to produce the well-defined phase probability that we know of as cross section. This piece is where all of the physics from our theory takes place, it tells us how we can go from some initial state to some final state and describes any intermediate interactions and particles that facilitate this *transition*. In the case of the fermion loop that supports the coupling of the Higgs to gluons, you encounter the following trace as described in Figure **2.3** and Equation (**2.2**),

$$N^{\mu\nu} = \mathrm{Tr}\left\{[\not{\ell} + \not{k}_1 + \not{k}_2 + m_q]\gamma^\nu[\not{\ell} + \not{k}_1 + m_q]\gamma^\mu[\not{\ell} + m_q]\right\} \ . \qquad (\mathbf{2.2})$$

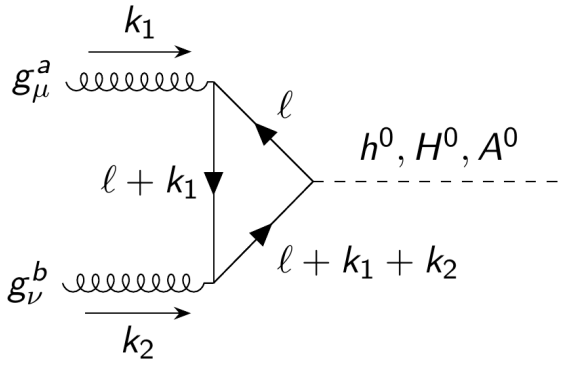

Figure 2.3: Feynman diagram for the gluon-gluon fusion production mode of the Higgs. Here the designations ℓ, k_1, k_2 refer to the momentum allocation for the fermion loop, initial state particles, and m_q is the mass of the fermion, either a top or bottom in this case.

Here, as discussed before in regard to the energy uncertainty, we have to integrate over the unknown fermion momentum, ℓ. Including the propagators associated with each fermion line we have to then evaluate the integral,

$$T^{\mu\nu} = \int \frac{d^N\ell}{(2\pi)^N} \frac{-2fN^{\mu\nu}}{\left[(\ell + k_1 + k_2)^2 - m_q^2 + i\epsilon\right]\left[(\ell + k_1)^2 - m_q^2 + i\epsilon\right]\left[\ell^2 - m_q^2 + i\epsilon\right]} \ , \qquad (\mathbf{2.3})$$

where we acquire a factor of 2 from being able to go clockwise or counterclockwise around the loop and a -1 from the nature of the closed fermion loop and account for the couplings and color factors in the f term. The N above denotes the dimensionality of the integral which we leave as arbitrary initially, $N = 4 + \epsilon$, and then take the limit of our solution as $\epsilon \to 0$. If we evaluate the trace, Equation (**2.2**),

we then obtain tensors as suggested by [33],

$$\begin{aligned} C_0 &= \int \frac{d^N\ell}{(2\pi)^N} \frac{1}{D_1 D_2 D_3} \\ C_1^\mu &= \int \frac{d^N\ell}{(2\pi)^N} \frac{\ell^\mu}{D_1 D_2 D_3} \\ C_2^{\mu\nu} &= \int \frac{d^N\ell}{(2\pi)^N} \frac{\ell^\mu \ell^\nu}{D_1 D_2 D_3} \end{aligned} \tag{2.4}$$

$$D_1 \equiv \left[(\ell + k_1 + k_2)^2 - m_q^2 + i\epsilon\right],\ D_2 \equiv \left[(\ell + k_1)^2 - m_q^2 + i\epsilon\right],\ D_3 \equiv \left[\ell^2 - m_q^2 + i\epsilon\right].$$

While C_0 is a scalar integral and can be evaluated explicitly, C_1 and C_2 are not and have to be to be reduced to scalar integrals through tensor reduction techniques. After applying the tensor reduction techniques, C_1 and C_2 can be written in terms of C_0 and the overall loop part of the matrix element for the production mode can be written as,

$$|T|^2 = -4f^2 \left[2 + (s - 4m_q^2)C_0\right] \tag{2.5}$$

2.4 Translating physics into code

Obtaining an analytic solution is one step in finally calculating the cross section and starting to look at what we can find out about these Flavor Changing Neutral Currents. The next step is no less daunting and involves developing computer calculations and code to generate these responses. Analyzing a signal and developing discovery potential plots requires us to calculate the signal and dominant physics background, and apply selection criteria to both to try and minimize contamination. Ultimately this comes down to a numerical integration technique with some dimensionality set by the complexity of the calculation. In

our case, there is not much to be gained by using higher level languages such as C++ and many of the libraries and programs we can use to help piece together the information are written in Fortran so that is the chosen language for the main code that we developed.

2.4.1 Code development and computational efficiency

The cross section code I developed with Baris Altunkaynak utilizes subroutines and refined functions to correctly interpret the physics and develop the integrals in such a way that we are always integrating under the limits of zero to one. In addition to analytically calculating the transition matrix element we also develop routines to calculate phase space for pair decays and calculate appropriate Jacobian factors.

The development of this code interface has allowed for better portability between systems which is ideal considering we utilize both our own personal hardware and the OU Supercomputing Center for Education and Research for many of our calculations. An additional advantage is the security of having one static 'cut' file where we can easily apply the same analysis to the signal and background codes by simply pointing it to the proper file to include. This improved my personal code integrity and allowed me to easily check calculations against other group members or software as described in the next section.

2.4.2 Consistency check

In order to check the accuracy of our calculations we compared results to those obtained from MadGraph, version 5, for preliminary or basic results, such as standard model Higgs production. We were able to achieve agreement within 1% of what MadGraph predicted, which we viewed as a more than acceptable margin.

MadGraph was then used to produce matrix elements for our background processes and interfaced these with our cross section code for consistency. Doing so also allows us to more easily control our selection criteria without having to rely on the limited options and algorithms employed by MadGraph. Once code techniques are verified and selection criteria are selected we can then move on to production and produce the data presented in this dissertation [34]. For analysis purposes we rely on programs such as Mathematica and ROOT to analyze and compare our signal data to our background data. ROOT analysis allows us to perform more realistic detector simulations but also requires us to use C++ language for calculation.

2.4.3 Theory versus phenomenology

In addition to high energy experiment and high energy theory there is a unique branch or classification of researchers known as phenomenologists. Phenomenology it a blend of the theoretical side of high energy physics and the experimental side and this is the category in which our research group is classified. Traditional high energy theory focuses mainly on the refining and development of new models to try and explain the world around us. In many scenarios this involves research that is more mathematically driven where you turn the knobs and dials of nature and see what all you can make within the parameter space you are given. String theory and some aspects of supersymmetry (SUSY) can fall into this category if the research's main focus is on model building.

Experimentalists on the other hand work directly with the data and often look at several theories simultaneously to see which one fits and describes the data best. Alongside theory, these two groups play a sort of cat and mouse style game where sometimes theory leads the discovery and sometimes the data leads to new theories. An example is the recent hint of a di-photon event excess at the LHC [35–38],

which spawned hundreds of new papers on the theory side trying to explain what might cause this excess. It turns out as more data was collected it was a statistical anomaly and not a new discovery but it still sparked a lot of interest. Contrary to that, discoveries of the top quark and Higgs boson were well heralded by theory which helped to direct the experimental searches and analysis to look for those particular signatures, [3, 4, 39].

Phenomenology is a unique approach where you play both roles as a theorist and experimentalist. Occasionally phenomenologists will analyze data from the LHC to support a study they are conducting. In our work we often try to implement the selection strategies used by the CMS and ATLAS collaborations to adequately model an experimental analysis. Instead of looking at data and trying to find the physics or building and perfecting models that have yet to be tested, we directly put models to the test in mock experimental settings so we can make predictions. At times this requires us to do a little model building ourselves but at the end of the day our goal is to still run simulations and try and look at the data like an experimentalist so we can tell them where to put their focus or offer suggestions on types of analyses they can conduct on their data to verify or disprove certain models. This requires us to have knowledge of the detectors, how they operate, and we need to be able to break down or expand the BSM theories and SM extensions that we wish to test.

Many of the studies we perform involve the utilization of several programs, many of which are modified to fit our needs, and developing our own framework for calculation. We also adopt several analysis criteria and methodologies from our experimentalist colleagues. One such criteria is the 5σ significance notion where we do not treat something as a discovery unless it has the proper statistical significance. Statistical significance, in this case, is determined by looking at how far above the standard background the signal + background event data lies. If the

signal 'bump' minus 2.5 times it's uncertainty lies at the edge of, or outside, the background plus 2.5 times its uncertainty, it is said to have a 5σ significance and counts as a discovery. Mathematically this can be represented by the following:

$$\sigma_S \geq \frac{n}{L}\left[n + 2\sqrt{L\sigma_B}\right] \tag{2.6}$$

or, in terms of number of events,

$$N_{SS} = \frac{N_S}{\sqrt{N_B}} = \frac{L\sigma_S}{\sqrt{L\sigma_B}} \geq 5 \ . \tag{2.7}$$

In Equation (**2.6**), $\sigma_{S,\ B}$ is the cross section of the signal + background and background only, respectively, and n is the scale parameter that selects how many standard deviations we are away from each datum. So, if we want a 5σ significance then we set $n = 2.5$ in to constitute a discovery. In Equation (**2.7**) ths is translated to a more familiar measure of the number of signal and background events, $N_{S,\ B}$ respectively. The conversion from cross section to number of events is straightforward, $N = \sigma \times L$ where, again, σ is the cross section (probability) and L is the integrated luminosity (amount of data collected).

Often times, as mentioned before, phenomenologists rely on experimental results to inform the studies we undertake. For instance, the idea to look at FCNCs as possible indicators of new physics beyond the SM was hinted by an excess of $h^0 \to \tau\mu$ events reported by CMS during their Run 1 analysis [30]. If these FCNC processes exist, they should be not only in the leptonic sector but also in the hadronic sector as they are both fermions and couple to the Higgs field

in similar ways. Since that interaction is directly proportional to mass,

$$\mathcal{L}_Y = -\frac{\lambda}{\sqrt{2}} \sum_{F=U,D,L} \overline{F}_L \Phi^0 F_R \tag{2.8}$$

where

$$\lambda \propto \frac{m_F}{v} \ , \tag{2.9}$$

where v is the Higgs vacuum expectation value, experimentally 246 GeV [23], then and FCNCs involving a Higgs interaction are likely to be seen most readily in an interaction between the top, charm, and Higgs. Since the top has a mass larger than that of the SM-like, light Higgs boson, $h^0 \to tc$ is not kinematically favorable. However, if we adopt a general 2HDM as discussed in Section 1.4, then a heavy Higgs, H^0, or pseudoscalar Higgs, A^0, decaying into a top charm pair is kinematically favorable for any masses more than twice m_t, or about 350 GeV. Furthermore, in a general 2HDM the heavier Higgs states FCNC couplngs are proportional to $\sin(\beta - \alpha)$ while the SM FCNC coupling is proportional to $\cos(\beta - \alpha)$ and current experimental results favor $\sin(\beta - \alpha) \to 1$. Our first approach to these rare decays then is to investigate the heavy Higgs sector and see if we can place constraints on the strength of the FCNC processes and make some predictions for what the LHC might see from that sector at higher energies and luminosities.

Chapter 3

Top, Charm, and Higgs, an Uncommon Trio

> "*What's in a name? That which we call a rose by any other name would smell as sweet*"
> — Romeo Montague, *Romeo and Juliet*, William Shakespeare

This chapter describes our first analysis of Flavor Changing Neutral Currents and is summarized in our publication, [40]. This chapter will serve as a more detailed analysis of this study, what it does, and why it is important. In regard to the famous line from one of Shakespeare's poems, scientists by and large have a very different opinion in regard to names and what they mean and, moreover, what they can tell you about an object. Turns our wizards and occult societies have the same opinion but hopefully that doesn't reflect poorly on us.

3.1 What's in a name?

The title of the paper we put out summarizing this result was *Flavor changing heavy Higgs interactions at the LHC* which tells certain readers quite a lot about the project. Let us take a moment to unpack that name a bit and get into what we're really looking at.

3.1.1 Flavor changing

As described earlier, the fundamental particle that make up matter as we know it involve quarks, leptons, and bosons. The quarks and leptons are divided into three generations and each type of quark or lepton is referred to as a flavor. Generally, when a neutral boson decays into two quarks it will decay into a

quark/anti-quark pair, like the dominant decay mode of the Higgs, $h^0 \to b\bar{b}$ [23]. In certain models like the 2HDM, however, we can get mixed decays from these neutral particles, such as an interaction between a Higgs, a top, and a charm. For a standard model Higgs, a Higgs with a mass of 125 GeV, the only possible way for this interaction to occur is through a top decay, $t \to ch^0$. If we relax the mass condition on the Higgs and allow it to be heavier than 125 or even 173 GeV, then $H^0 \to t\bar{c}$ and $H^0 \to c\bar{t}$ become possible. This is the heavy Higgs range.

3.1.2 Heavy Higgs interactions at the LHC

As mentioned above, heacy Higgs refers to Higgs bosons that have a mass larger than that of the currently observed, Standard Model-like Higgs boson. If you recall, when we added a second doublet to the Higgs sector then we actually generated four additional Higgs bosons which we denoted: H^0, A^0, $\mathrm{H}^{\pm}$. The CP-Even scalar, H^0, we assume to be heavier than the one we have already discovered and so designate it as the heavy Higgs. The CP-odd pseudo-scalar A^0 is our other neutral Higgs boson which we designate as the pseudo-scalar. In cases where m_{H^0} and $m_{A^0} > m_t = 173$ GeV, then the decays listed above, H^0 / $A^0 \to ct$ are now possible. These are the decays that we choose to study.

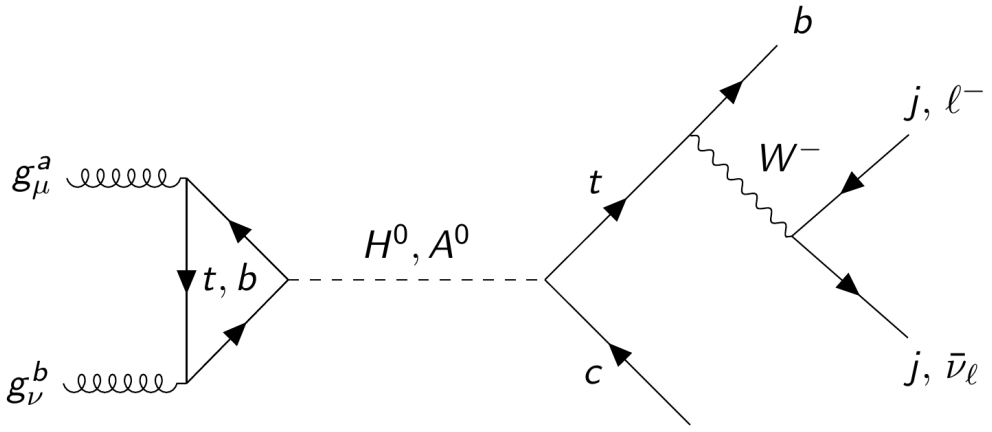

Figure 3.1: Feynman diagram for the $\phi^0 \to tc$ process where we define $\phi^0 = h^0$, H^0, A^0. We look at both the $W \to jj$ and the $W \to \ell\nu$ final states to maximize our signal strength.

3.2 Strangers in a strange land

Now, one might wonder, if a decay of $t \to ch^0$ is possible, why haven't we seen it yet, and furthermore, what is hoped to be gained by this study. To answer the first question we need to look at how particles couple in the SM. For starters, let me remind you we are dealing with fields and as such all of the operators and couplings that govern how these fields operate are tensors of some form or another. As it happens, all of our experimental evidence so far supports the construction of the yukawa couplings in the Higgs sector, in the sense that they are all diagonal. The interaction Lagrangian for the Yukawa couplings is as follows,

$$\mathcal{L}_Y = -\frac{1}{\sqrt{2}}\overline{U}\kappa_u h^0 U \ , \tag{3.1}$$

where $\psi_{L,R}$ refer to the fermion fields, h^0 is the SM Higgs field, and the κ_u term is defined as:

$$\kappa_u \equiv \begin{pmatrix} \kappa_{uu} & 0 & 0 \\ 0 & \kappa_{cc} & 0 \\ 0 & 0 & \kappa_{tt} \end{pmatrix}. \tag{3.2}$$

In this coupling matrix the terms along the diagonal are the same flavor couplings and the off-diagonal elements describe the strength of the flavor mixing couplings. Since they are all zero in the SM these couplings are forbidden at the tree level. They can exist as loop processes, Figure **3.2**, but those are higher order processes and are less favorable in general as well as being further suppressed by the GIM mechanism, [27].

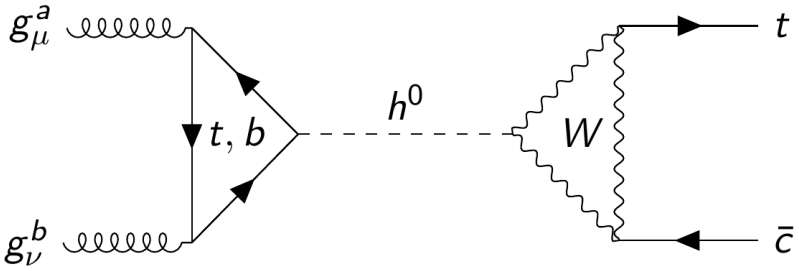

Figure 3.2: Feynman diagram for the $h^0 \to tc$ loop process that allows for FCNCs in the SM. Not shown are the decay modes of the top in this diagram but they would be the same as in the previous figure.

With this in mind, we can safely say that any signatures of a FCNC process would indicate something beyond the SM. Furthermore, by looking at these processes in the context of a general 2HDM we can gather information about how an extended Higgs sector operates. This is specifically important as many of the predominant beyond SM theories SM rely on such an extension, [17, 41]. The advantage of a general treatment, however, is that we do not require some of the

more restrictive assumptions in more complete models. While this does limit our ability to analyze and predict other beyond the SM (BSM) properties and effects it allows our findings to be more versatile and adaptable to the different models we may want to look at.

When we adopt a general 2HDM we gain several key advantages. First, we can now see FCNCs at the tree level as shown in Figure **3.1** due to the fact that we now have a new Lagrangian that describes our interactions,

$$\begin{aligned}\mathcal{L}_Y = &-\frac{1}{\sqrt{2}}\sum_{F=U,D,L}\bar{F}\left[\left(\kappa^F s_{\beta-\alpha}+\rho^F c_{\beta-\alpha}\right)h^0+\left(\kappa^F c_{\beta-\alpha}-\rho^F s_{\beta-\alpha}\right)H^0\right]F\\ &+\frac{1}{\sqrt{2}}\sum_{F=U,D,L}\bar{F}\left[i\,\mathrm{sgn}(Q_F)\rho^F A^0\right]P_R F \qquad (\mathbf{3.3})\\ &-\bar{U}\left(V\rho^D P_R-\rho^{U\dagger}V P_L\right)DH^+-\bar{\nu}\left(\rho^L P_R\right)LH^+ + \text{H.c.}\ ,\end{aligned}$$

where U, D, and L are the up-type quarks, down-type quarks, and leptons respectively; $c_{\beta-\alpha} \equiv \cos(\beta-\alpha)$; and $s_{\beta-\alpha} \equiv \sin(\beta-\alpha)$. As can be seen in the Lagrangian above, we have coupling terms to both h^0, our SM-like Higgs, and the new Higgs bosons, H^0 and A^0. In order for the experimentally verified SM to hold we need this new Lagrangian to reproduce SM results while retaining the ability to produce these new effects. The limit in which Equation (**3.3**) becomes Equation (**3.1**) is called the alignment limit. In the context of our model, we reach this limit as $\sin(\beta-\alpha) \to 1$ by allowing the κ^F matrix to be equal to the SM κ matrix. This also means that all of our FCNC information is stored in the ρ^F matrices.

Once again, the model we are using is a general 2HDM so there are no additional simplifying assumptions we can make about the couplings or constraints. For this study, valid parameters that must be considered are the value of $\cos(\beta-\alpha)$ and the diagonal parameters of the ρ^F matrix: ρ_{tt}, ρ_{bb}, ρ_{cc}, and $\rho_{\tau\tau}$. In addition, to to the freedom granted by not imposing additional symmetries we are also not required

to be Hermitian in the Yukawa part of the Lagrangian. In practice, this means that the off diagonal terms, ρ_{tc} and ρ_{ct}, can be very different from one another. In our case this is actually a very helpful scenario as ρ_{ct} is heavily constrained by the CKM matrix, [42, 43], but ρ_{tc} is not bound by the same constraints. In the context of the neutral Higgs bosons, since they are scalars and pseudo-scalars they have no chirality preference which allows us to adopt a funny *effective* coupling combining the two:

$$\widetilde{\rho}_{tc} = \frac{1}{\sqrt{2}}\sqrt{\rho_{tc}^2 + \rho_{ct}^2}\ . \tag{3.4}$$

3.2.1 Good news and bad news

The scene is set for our foray into FCNCs as a method for studying the presence of a second Higgs doublet in the most general sense. Now, how does one study a FCNC process and how do you know if what the signal you are detecting is indeed a FCNC process or not?

The benchmark of the signal we are looking for is some top and charm pair coming from a single resonant particle. Tops are not very long lived and so they are likely to decay and the dominant mode for that decay is into a b quark and a W boson. The W boson, like the top, does not generally stay around for too long and also decays. About 33% of the time the W will decay into a lepton and a neutrino, say an e or a mu, but another 67% of the time it will decay hadronically into quark/anti-quark pair like a $u\bar{d}$ for instance. At detectors, these decay products are all that survive and are visible in the context of analyzing your process. The main challenge with any decay process you want to study is then with picking out the signal of interest when there are other processes producing the same final set. We can control this issue in a couple of ways, one of which is

selecting decay modes that are unique in some way and thus do not have a lot of background contamination. On that note, we actually chose to study the leptonic decay mode of the W for our signal as any signal involving 3+ jets generally has a large background from $t\bar{t}$ production and general QCD processes. The other method of controlling background contamination is to use what are called selection rules. How selection rules work, is they exploit physical properties of your signal that your background is either incapable of producing or exhibits these properties at an acceptable rate.

3.2.2 Tools of the trade

As mentioned before, the two big tools we have in our toolbox is carefully selecting our decay modes and controlling how we analyze the data to favor our signal over the background. As phenomenologists we also want to make sure our data sets and analysis reflect the techniques and methods used at the detectors by experimentalists. In a typical bunch crossing there are roughly 40 million events [44], of which only about 1% of that is actually readout and collected due to simple limitations of space and readout speed. When a collision occurs the collision and decay information passes through very sophisticated trigger systems the allow the LHC collaborations to pick out *interesting* behavior. Part of the selection rules we use then are to match the LHC triggers used by ATLAS and CMS [44, 45]. For our particular process we implemented the cuts listed in Table **3.1**.

L = 25[a], 30[b] fb^{-1}	L = 300 or 3000fb^{-1} [c]
$\not{E}_T > 20$ GeV	$\not{E}_T > 40$ GeV
$p_T(j) > 20$ GeV	$p_T(j) > 30$ GeV
$\epsilon_b = 60\%$, $\epsilon_c = 14\%$, $\epsilon_j = 1\%$	$\epsilon_b = 50\%$, $\epsilon_c = 14\%$, $\epsilon_j = 1\%$
$p_T(\ell) > 20$ GeV	
$\lvert\eta_\ell\rvert$, $\lvert\eta_j\rvert < 2.5$	
$\lvert m_{b\ell\nu} - m_t\rvert < 0.20 m_t$	
$\lvert m_{b\ell\nu c} - m_\phi\rvert < 0.20 m_\phi$	
$0.85 p_c < p_T(c) < 1.10 p_c$	

Table 3.1: We require exactly 1 lepton to meet the $p_T(\ell)$ cut above and exactly 1 b-tagged jet and 1 non b-tagged jet to meet the $p_T(j)$ cut listed. The charm momentum, p_c, for the signal and background is found according to Equation (**3.5**) and $\not{E}_T$ is calculated by adding up all the visible particle momenta.

The efficiencies listed above ($\epsilon_{b,c,j}$) are the frequencies at which the particle of interest is tagged as a b-jets. We refer to these as tagging, ϵ_b, and mistagging, $\epsilon_{c,j}$ efficiencies. The top three rows are specific to the integrated luminosity of the detector; 25 and 30[b] fb^{-1} or 300[b], and 3000[a] fb^{-1}; while the rest are applied for all luminosities.

$$p_c = \frac{m_\phi}{2}\left[1 - \frac{m_t^2}{m_\phi^2}\right] \tag{3.5}$$

In the formula and table above, m_ϕ is the mass of the Higgs boson taking part in the decay. In this study, either a heavy Higgs boson, H^0, or the pseudo-scalar Higgs, A^0. The cuts in Table **3.1** are chosen to both represent what has been done at the detectors before through trigger levels and searches that constrain our signal,

[a] $\sqrt{s} = 8$ TeV
[b] $\sqrt{s} = 13$, 14 TeV
[c] $\sqrt{s} = 14$ TeV

[45, 46], and from our own analysis of signal versus background events. In addition to background processes that mimic the final state that we are trying to detect there are also built-in restrictions due to the nature of the particle themselves that can hinder such a search.

3.2.3 Rules of the realm

The hindrance in the heavier Higgs states has to do with how likely they are to decay into the state we want in the first place. Figure **3.3** shows the dominant decay modes of both the heavy Higgs scalar and the pseudoscalar. When the masses of these new particles are around that of the SM-like or light Higgs boson our tc decay mode actually dominates but becomes less significant as the mass increases above twice m_t. In our case, the $t\bar{t}$ background can be reduced with the cuts we apply for this study seeing as at minimum a $t\bar{t}$ even would produce a final state with either 2 b-jets and 2 leptons, or 2 b-jets, 2 light jets, and an isolated lepton, both of which violate our event selection criteria. This means for us, then that we do not have to worry about much contamination from ancillary Higgs decay processes but we still have significant SM backgrounds we need to analyze, the strongest of which is the W + jets background.

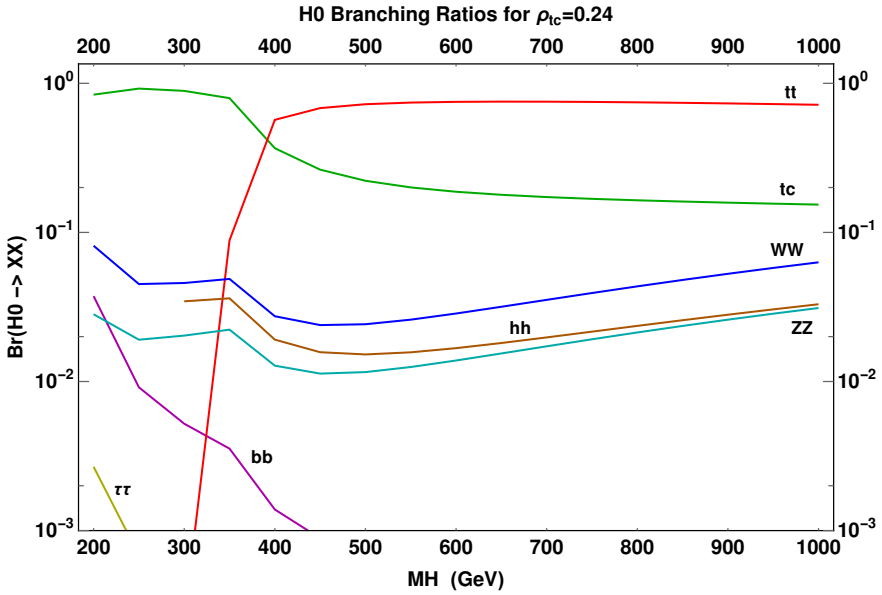

(a) M_H branching ratios obtained using 2HDMC.

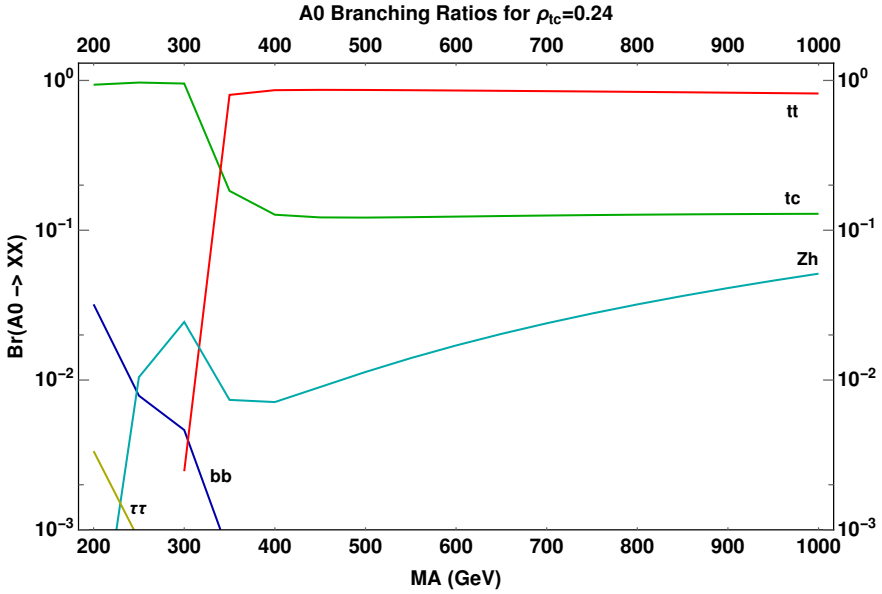

(b) M_A branching ratios obtained using 2HDMC.

Figure 3.3: Branching fractions of (a) the heavier Higgs scalar, H^0 and (b) the Higgs pseudoscalar, A^0 as a function of Higgs mass, m_ϕ, with $\cos(\beta - \alpha) = 0.1$, $\widetilde{\rho}_{tc} = 0.24$, and $\rho_{ii} = \kappa_i$ for the diagonal couplings.

The branching ratios depicted in Figure **3.3** show a best case scenario for a $\widetilde{\rho}_{tc}$ coupling to be at the ATLAS sensitivity level [47] that can still be consistent with the alignment limit. Some of the striking features are the sharp breaks around 300 GeV and the non-existence of an $H^0 \to h^0 h^0$ decay mode before then. In the case of the sharp break around 300 GeV this corresponds to decays into real $t\bar{t}$ pairs being kinematically favorable once your resonant mass reaches $2 * m_t \approx 350$ GeV. In the plots above, only the decay modes that produce direct background than are signal and so do not appear on the plots above.

We also must take into account the strength of the background processes that mimic our final state. One of our best discriminating tools in this case is applying the cuts that were highlighted in Table **3.1**. In the case of this search the Higgs mass window had the largest effect at reducing the background when coupled with the cut on the charm momentum. The p_T and $|\eta|$ cuts for more for eliminating contamination from low energy electroweak processes and $t\bar{t}$ pair production. The most significant background was still in the W + jets channel which could be an electroweak process or could be produced through a single top. Additional contamination from $t\bar{t}$ processes where one of the b-jets was misidentified, one W decays leptonically, and the other W decays into two soft jets that do not pass our p_T cuts. The tight requirements for the $t\bar{t}$ channel allowed us to effectively eliminate or at least reduce the otherwise overwhelming production rate to a process on the order of our signal event. Figure **3.4** shows the cross sections of the signal and background processes as a function of heavy Higgs mass for the $H^0 \to tc$ decay.

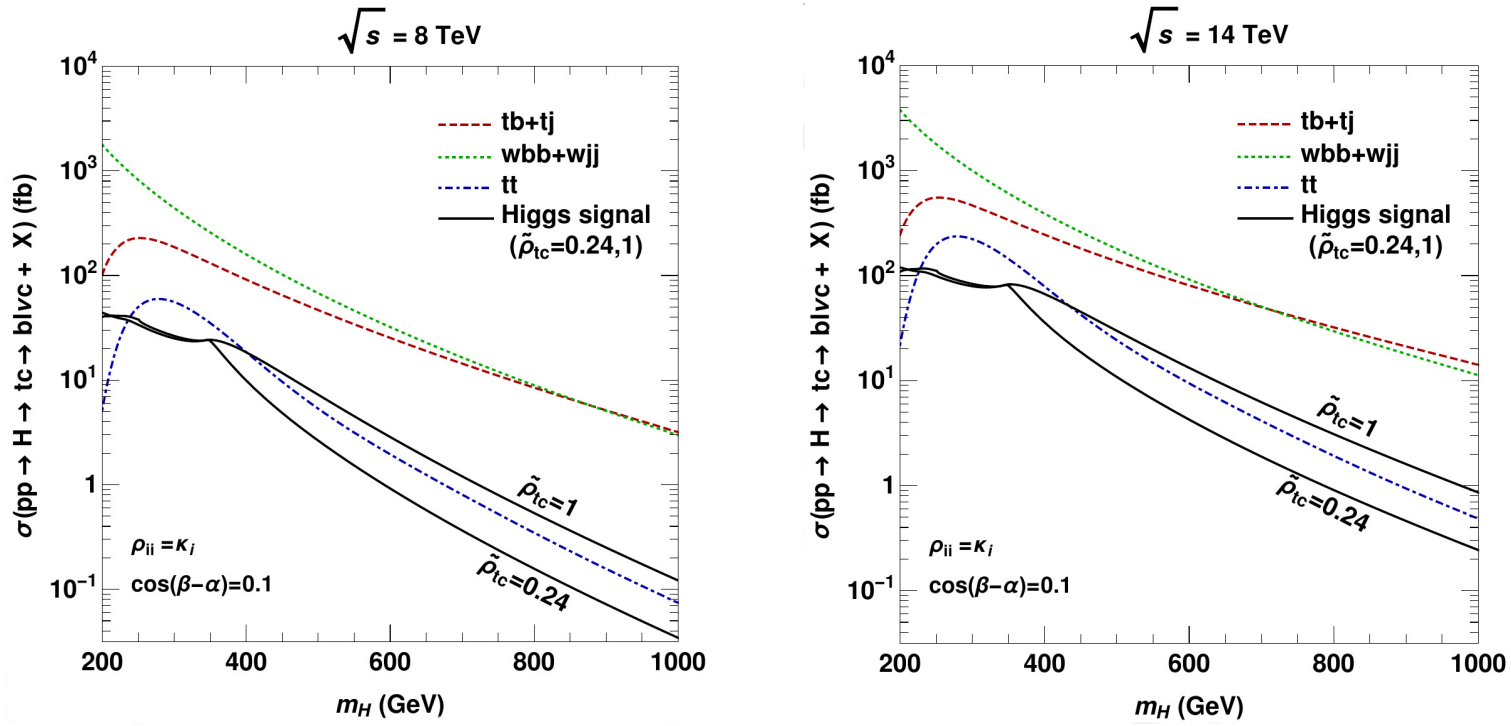

(a) Cross section and dominant SM background at $\sqrt{s} = 8$ TeV.

(b) Cross section and dominant SM background at $\sqrt{s} = 14$ TeV.

Figure 3.4: The cross section of the heavy Higgs scalar, H^0 (solid, black) for $\sigma(pp \to H^0 \to t\bar{c} + c\bar{t} \to bj_c\ell\nu + X)$ at the LHC as a function of mass, m_H. Results are shown for bench mark values of $\widetilde{\rho}_{tc} = 0.24,\ 1.0$ for $\sqrt{s} = 8,\ 14$ TeV with a fixed $\cos(\beta - \alpha) = 0.1$. For th background processes shown (dashed lines), we have applied all selection rules, appropriate K-factors, and tagging efficiencies.

3.3 Proclamations and predictions

The test of any good theory is how well it makes predictions and what those predictions can tell us. As discussed in Section 2.4.3, a measure that both experimentalists and phenomenologists use to determine a discovery is statistical significance, Equation (**3.6**),

$$N_{SS} = \frac{N_S}{\sqrt{N_B}} \geq 5 \ . \tag{3.6}$$

After all cuts and tagging efficiencies our signal is still roughly two orders of magnitude below our background but that is not as concerning due to the proportionality of N_S to $\sqrt{N_B}$. From this information we are able to then find projections of what values of $\widetilde{\rho}_{tc}$ are accessible through searches at the LHC. Also, keep in mind, even if we do not see anything necessarily does not mean it is not there. It is well accepted that the dominant branching ratio of the SM-like, light Higgs, h^0 is to a $b\bar{b}$ pair which is just now reaching the point where it might be accessible through direct searches [23]. In many of these cases we simply need more data, higher integrated luminosities, to drive down our statistical uncertainties and enhance these rare signal events.

Using the satistical significance criteria and analyzing our signal over a range of different viable $\widetilde{\rho}_{tc}$ values allows us then to predict what $\widetilde{\rho}_{tc}$ should produce a 5σ result based on the anticipated luminosity values a the LHC; 30, 300, and 3000 fb^{-1} [48]; and the possible mass of the heavier Higgs state. For these calculations we assume a degeneracy in all of the heavy Higgs masses allowing $m_H \approx m_A$,

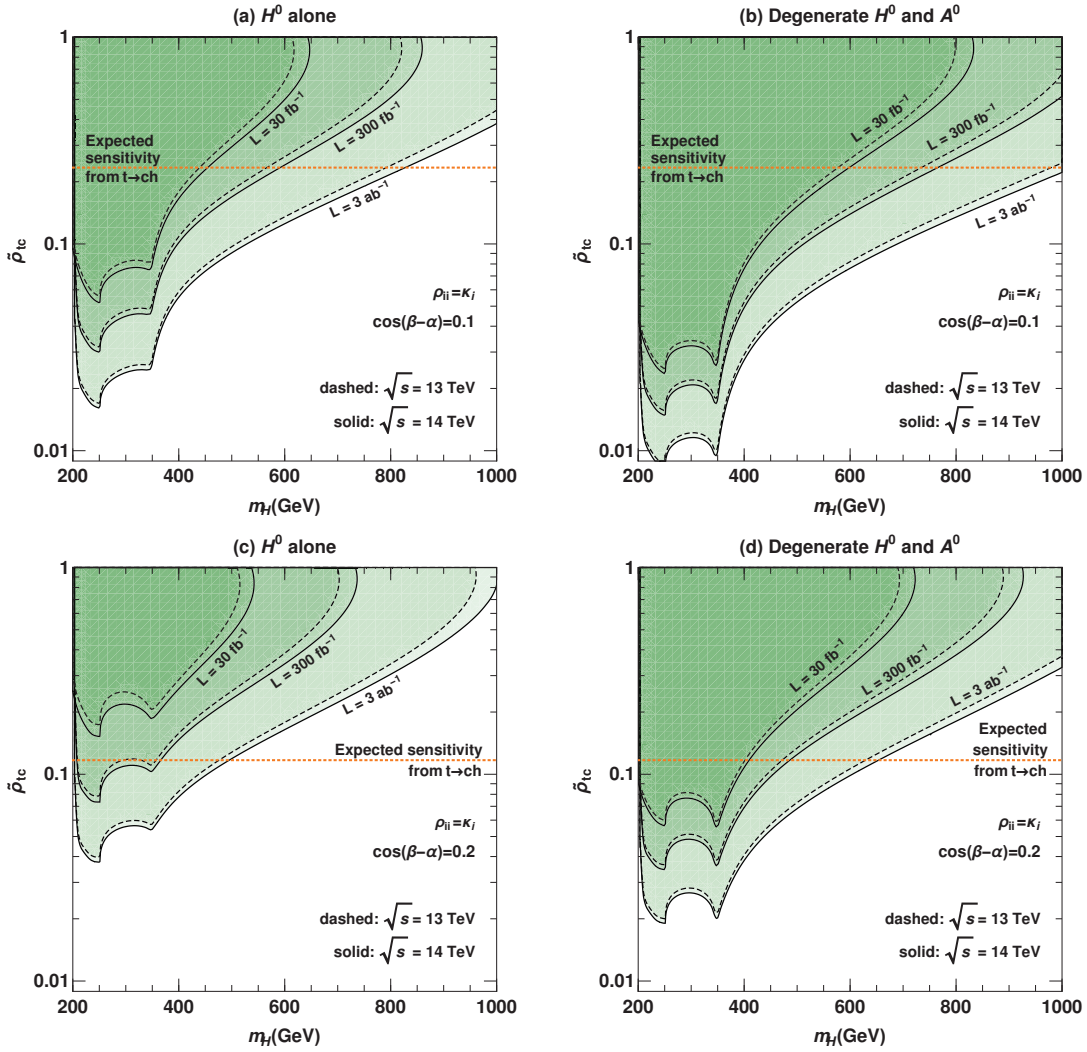

Figure 3.5: Discovery potential for a 5σ significance in the $m_\phi - \widetilde{\rho}_{tc}$ plane for the $\sigma(pp \to H^0 \to t\bar{c} + c\bar{t} \to bj_c\ell\nu + X)$ signal at LHC center of mass energies, $\sqrt{s} = 13$ (14) TeV, the dashed (solid) contours. (a) and (c) are discovery potentials for the heavy, H^0, Higgs alone while (b) and (d) show combined results for both H^0 and A^0. In (a) and (b) $\cos(\beta - \alpha) = 0.1$ while we relax that constraint in (c) and (d) and allow $\cos(\beta - \alpha) = 0.2$. The shaded regions above the contours indicate the favorable parameter space for $\widetilde{\rho}_{tc}$ given the 5σ discovery criteria we used to construct the curves.

What we find with these discovery potentials is that we have a considerable parameter space in which we can hope to find evidence of flavor changing neutral currents involving the production and decay of heavy Higgs states that accompany

extending the Higgs sector of the SM with a second Higgs doublet. This is done in a general two Higgs doublet model where we specifically do not place any hard constraints on how the two doublets should interact and only require that we can reproduce observed SM results in the alignment limit as $\sin(\beta - \alpha) \to 1$. Much of the parameter space will be swept out by the end of Run 2 but there is some viable parameter space that may not be accessible until after the high luminosity upgrade is completed and new data is collected.

Our basis for this research was in some way rooted by the excess of FCNCs reported by CMS in Run 1 in the $h^0 \to \tau\mu$ channel [30]. However, 2HDMs are prominent in many extensions of the SM including supersymmetry which requires a Type-II 2HDM where one Higgs doublet preferentially couples to up-type quarks and the other to down-type quarks. If we discover these events, that may then give us some insight into the structure of such a 2HDM which can help narrow down what BSM theories might be governing the global picture. We also chose to look at the $\phi^0 \to tc$ case due to its strong coupling to the Higgs field and relatively straight forward analysis. While $h^0 \to \tau\mu$ events have been reported at some significance the analysis and process of producing event data for those decays takes considerable more effort as described in the next chapter on our analysis or leptonic FCNCs with $\tau\mu$ events.

Chapter 4

When the Higgs Meets the Tau and the Muon

"*You cannot hide, I see you!*"
— Sauron, *The Lord of the Rings*, J.R.R. Tolkien

The Higgs interaction with the tau, τ, and the muon, μ, was our first experimental indication that FCNC processes may be visible at the LHC. The excess announced by CMS during Run I was only a 2.4σ significance, so not nearly enough to constitute a discovery, but was enough to give us a hint at where we should look. In addition, this would be the first FCNC process kinematically accessible by a SM-like Higgs with a mass below the top mass, m_t. The SM-like or light Higgs, h^0, still has a $\cos(\beta-\alpha)$ factor that reduces the visibility of a $\tau\mu$ signal so it is also prudent to consider the heavier Higgs states, H^0 and A^0, as they are proportional to the complimentary $\sin(\beta-\alpha)$ term.

4.1 Leptonic FCNC processes

The overall process of a Higgs field coupling to a tau and muon, $\phi \to \tau\mu$ where $\phi = H^0,\ A^0,\ h^0$, is not fundamentally any different than the Higgs field coupling to the top and charm, Equation (**1.40**). It is still the off-diagonal elements of the ρ^F, or in this case $\rho_{\tau\mu}$, that generate these flavor changing states. One important difference between the htc coupling and the $h\tau\mu$ coupling is the $\tau\mu$ state is a viable decay for the SM Higgs process and we do not need to wait for a more massive particle to see such an interaction. Unfortunately, such a decay is suppressed as we approach the alignment limit by the $\cos(\beta-\alpha)$ term. In addition, since the τ and μ are so light their coupling to the Higgs field is not as strong as the heavy

quark states, charm and top. Figures **4.1**(a) and **4.1**(b) illustrate how favorable such a decay is in the context of the other possible channels. In Figure **4.1**(a) we scan over possible values of the heavy Higgs particle much as was done in the *htc* study. In Figure **4.1**(b), however, since the mass of the Higgs boson is fixed by observation at 125.2 ± 0.24 GeV [a], we scan over possible $\rho_{\tau\mu}$ values instead.

[a] http://pdglive.lbl.gov/Particle.action?node=S035&init=0

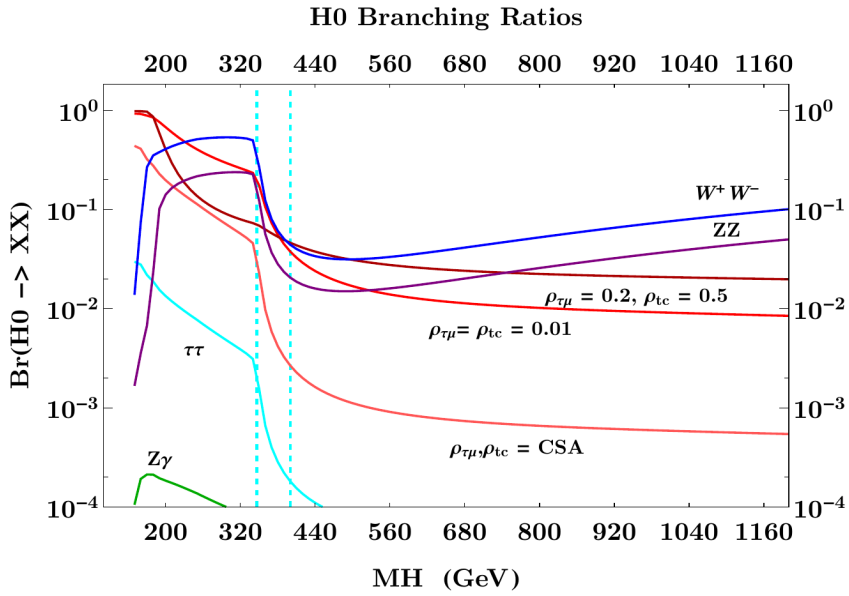

(a) M_H branching ratios obtained using 2HDMC.

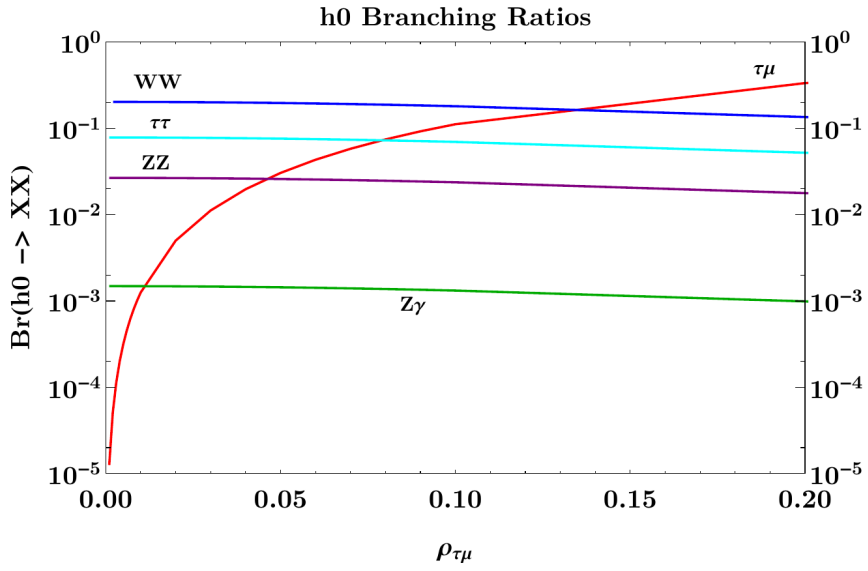

(b) M_h branching ratios obtained using 2HDMC.

Figure 4.1: This figure shows the branching ratios of (a) the heavy Higgs scalar, H^0, for a range of Higgs masses. Included are curves for several test values of the $\rho_{\tau\mu} = 0.2,\ 0.01$, and 2.489×10^{-2} (CSA). In (b) the branching fractions of the SM-like Higgs are shown as a function of the $\rho_{\tau\mu}$ coupling as the mass was fixed at 125.1 GeV. Here, in (a), preference has been given to show alternative Higgs decays that may serve as background to $\phi^0 \to \tau\mu$ signal, where $\phi = H^0,\ A^0,\ h^0$.

Normally, all branching fractions will add up to unity collectively, in Figure **4.1**(a), the $H^0 \to tt$, the $H^0 \to tc$, $H^0 \to bb$, and the $H^0 \to h^0h^0$ are not shown, which is why the plot only shows values up to 0.1 or 10%. Due to this choice, all decay processes involved here do not encompass the main decay modes of H^0 so even if ρ_{tamu} were to be high, it would still be considered a rare process. The advantage of the lepton sector, however, is it does not have as much background from QCD processes.

4.2 Interplay between the $\phi \to tc$ and $\phi \to \tau\mu$

In addition to the background processes generated from the heavy Higgs scalar, H^0, we also have to take into account the $\phi \to tc$ flavor changing processes. In some ways this is an addendum to our work in [40] with the added complexity associated with decaying tau particles. Since we are using a general 2HDM still, FCNC processes, if present, are at the tree-level and add another decay channel to the particle states with masses $\geq m_t = 173.2$ GeV. Including additional decay modes in the heavier Higgs states causes their decay width, the sum of all of their decay modes, to change as well. In order to accurately make calculations and predictions for $\phi \to \tau\mu$ signal we then have to include information about ρ_{tc}. As no observations of a $H^0, A^0 \to tc$ signal has been reported yet, we have no experimental benchmark values to report. As reference we chose to use a conservative value chosen as a case study in [40] of $\rho_{tc} = 0.1$.

Since $h^0 \to tc$ decay is considered inaccessible, the choice of ρ_{tc} does not have an effect on the SM, or light Higgs, decay width. The $h^0 \to \tau\mu$ decay, however, is accessible and has a profound impact on the SM Higgs width and must be treated with some care. In addition to constraints placed on the coupling by looking at BABAR [49] and Belle II [50] data for $\tau \to \mu\gamma$ that say $\rho_{\tau\mu} \leq 0.26$, we also must

consider how much deviation from the reported SM Higgs width is acceptable.

$\rho_{\tau\mu}$	2.489×10^{-2}	0.1	0.2	0.26
Γ_h	3.991×10^{-3}	4.45×10^{-3}	5.95×10^{-3}	7.324×10^{-3}
$g_{h\tau\mu}$	1.76×10^{-4}	7.10×10^{-3}	1.40×10^{-2}	1.83×10^{-2}

Table 4.1: This table shows the SM Higgs width, Γ_h calculated from 2HDMC, as a function of $\rho_{\tau\mu}$ with $\cos(\beta - \alpha) = 0.1$ and $\rho_{tc} = 0.1$. The $g_{h\tau\mu}$ terms show the coupling to the Higgs field, accounting for all other coefficients, as shown in Equation (**4.1**).

The table shown above highlights the impact that changing $\rho_{\tau\mu}$ has on the h^0 decay width, Γ_h. Also reported in that table are values for the adjusted Higgs coupling which takes into account the value of $\rho_{\tau\mu}$ and $\cos(\beta-\alpha)$ in the Lagrangian,

$$g_{h\tau\mu} \equiv \frac{\rho_{\tau\mu}\cos(\beta-\alpha)}{\sqrt{2}}\,. \tag{4.1}$$

Based on the constraints of [49, 50] and the results shown in Table **4.1** case studies were chosen for $\rho_{\tau\mu} = 2.489 \times 10^{-3}, /0.1,$ and 0.2 keeping us within 1%, 12%, and 40% of the reported width respectively. A discrepancy from the observed SM width of 40% is quite extensive and is not viewed as a realistic assumption but will serve to provide upper-limits on coupling strengths for this study.

4.3 Decaying the τ

Generally speaking, particle decays are very formulaic. You generate Feynman diagrams to explain the physics of the process, obtain the Feynman rules for each vertex, compute the trace, evaluate the phase space, and compute the integral. This process does not change much with the tau, but it does get slightly more

complicated. Like the top, the tau is the heaviest lepton with a mass or around 1.77 GeV[a]. This means a couple things. First, the decay of a tau into another lepton is possible. Second, it can decay into a hadron, specifically a meson that contains a quark anti-quark pair.

If the tau decays hadronically, the subsequent meson will most likely cause a shower in the hadronic calorimeter which will cause the tau to look like a funny jet, aptly name a tau-jet. Dealing with jets in a detector simulation usually is not very hard, it gets tagged as a jet and from a theory standpoint we don't need to know much more than that. With a tau-jet, however, the particulars of the jet can depend heavily on which meson the tau decayed through, either a π, ρ, or $a1$. All three decay modes then have to be taken into account to accurately model the hadronic tau decay mode.

The leptonic decay mode is more straightforward, the tau decays into a virtual W which then decays into either a $\mu\nu_\mu$ or an $e\nu_e$ with nearly the same frequency, 10.6% and 10.7% respectively. In this study, to reduce contamination, we are mainly interested in the electron/positron final state as that then gives us to different flavor leptons in the final state. With that in mind, we do take special care to use the properties of the electron tau decay instead of a more generic lepton decay that could be either an e or a μ.

In addition to the challenges associated with the decay of the tau, production of the tau presents its own challenges, especially in this $\tau\mu$ process. The SM-like Higgs has a mass of 125.1 GeV and we expect the heavy Higgs and pseudoscalar Higgs to be even heavier still. The muon and tau by contrast have a collective mass of about 1.883 GeV. Because of this large mass difference, the tau and muon generated from the event are highly boosted, meaning they are traveling more or less along the same path as the parent particle, instead of scattering at new

[a]http://pdglive.lbl.gov/Particle.action?node=S035&init=0

angles. Likewise, the tau decay products are also going to be highly boosted which causes problems when the event is reconstructed. In order to get a picture or what happened we have to employ the collinear approximation [51] where we use information about the parent particle and the momentum deposited in the transverse plane after the tau decay to effectively construct the momentum of parent tau. For the muon this is not necessary since it is already a final state particle, but the tau will decay and so we need to know the four momentum it had to accurately reconstruct the event.

The collinear approximation essentially says that the decay product will simply carry some fraction of the parent particle's momentum but be in the same direction, hence the col in collinear. Mathematically this means

$$P(\ell, j) = \chi_{\ell,j} \cdot P(\tau)\,. \tag{4.2}$$

Likewise, there will be some missing transverse momentum from a tau neutrino, ν_τ, that will carry the rest of the parent momentum

$$\not{E}_T = (1 - \chi_{\ell,j}) P_T(\tau)\,, \tag{4.3}$$

where $\chi_{\ell,j}$ represents the momentum fraction the lepton or hadron (j) has from the parent tau, $P_T(\tau)$ denotes the transverse momentum of the tau, and $P_{\ell,j}$ represents the momentum of the decay product of the tau. In the situation above, it is the $P(\tau)$ and the $\chi_{\ell,j}$ that are not known but $P(\ell, j)$ and $\not{E}_T$ are final state values that would be measured at the collider. We then rely on the tried and true system of equations method where we can combine these two equations to effectively

reconstruct the momentum of the parent tau

$$P(\tau) = \frac{P(\ell, j)}{\chi_{\ell,j}}\,, \tag{4.4}$$

where

$$\chi_{\ell,j} = \frac{P_T(\ell, j)}{P_T(\ell, j) + \not{E}_T}\,. \tag{4.5}$$

This allows us then to know the most probable four momentum for the parent tau and will let us more accurately produce the reconstructed Higgs that produced the tau and muon pair.

4.4 SM physics background

As with any signal search in particle physics, there is more than one way our select final state can be produced. The challenge then is tuning your analysis to pick out your signal over the background without making too many assumptions. The $\phi \to \tau\mu$ signal is no exception and also provides us with some interesting challenges. For the signal in this case, since we are looking at both the hadronic and leptonic decay modes of the tau, we have to include the backgrounds associated with each process. In addition, as is indicated in Figure **4.1**(a), there are several possible decay products of a heavy Higgs scalar that need to be accounted for.

4.4.1 Hadronic τ backgrounds

For the hadronic decay of the tau we are looking for a muon and associated jet that is highly boosted. This same final state can also be produced from an intermediate Wj process where the W decays to a muon and a muon neutrino, $\mu\nu_\mu$ that comes from either a single top or an electroweak particle like a photon, γ, or

a Z. If we first produce a pair of taus, $\tau\tau$, and we allow one to decay hadronically into a jet and the other to decay leptonically into a muon, then this will also produce similar kinematics to our signal. A very similar background process exists if we consider a WW intermediate process where one W decays into a $\mu\nu_\mu$ and the other decays into a tau that then decays hadronically and so will be tagged as a jet.

$\sigma(pp \to X)$	$\sqrt{s} = 8$ TeV	$\sqrt{s} = 13$ TeV	$\sqrt{s} = 14$ TeV
$pp \to WW \to \tau\mu$ hadronic	0.9145 fb	1.5188 fb	1.6245 fb
$pp \to \tau\tau$ hadronic	37.2235 fb	58.7502 fb	62.8659 fb
$pp \to Wj \to \mu\nu_\mu\, j$	4.4804×10^2 fb	8.0711×10^2 fb	8.8093×10^2 fb

Table 4.2: This table shows the hadronic background cross sections for the $\phi \to \tau\mu$ signal with $M_H = 125.1$ GeV. Here we have already applied our selection rules for the signal that will be further discusses in Section 4.5.

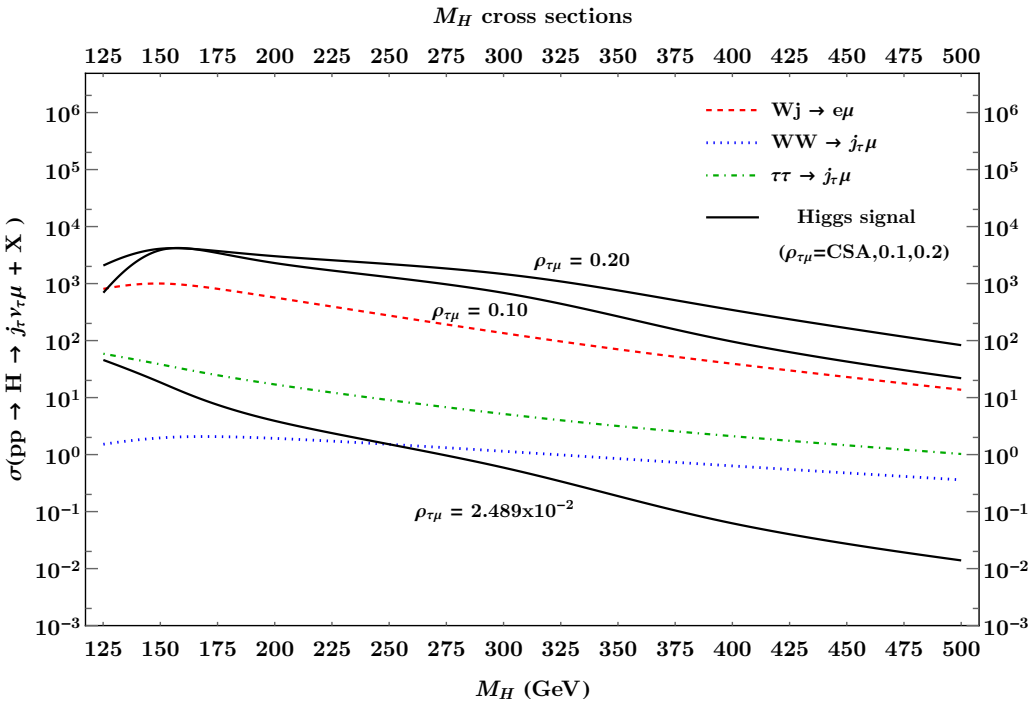

Figure 4.2: Here the SM background for the hadronic decay process at $\sqrt{s} = 13$ TeV is shown as it compares to the signal cross section after full selection cuts. The black curves show the cross section as a function of $M_H \in [125, 500]$ GeV for the various case studies of $\rho_{\tau\mu}$ that were selected: 2.489×10^{-2}, 0.10, 0.20; for $\rho_{tc} = \cos(\beta - \alpha) = 0.1$.

4.4.2 Leptonic τ backgrounds

In the leptonic sector we have to contend with even more background processes than we did than with the hadronic decay mode. Furthermore, we have to be cautious as to which type of lepton the tau decays into. If the tau decays into another muon then we have backgrounds from ZZ and $Z\gamma$ final states, if we do not we can avoid those backgrounds. Shown below, Table **4.3**, is a table showing the dominant background processes for the different flavor ($e\mu$) lepton final state and same flavor lepton final states will be added later in this work. For the $e\mu$ final state the dominant background processes are WW, $\tau\tau$, and $WW \to \tau\mu$. In

each case, one particle decays into the muon we expect and the other decays into an electron.

$\sigma(pp \to X)$	$\sqrt{s} = 8$ TeV	$\sqrt{s} = 13$ TeV	$\sqrt{s} = 14$ TeV
$pp \to WW \to \tau\mu$ leptonic	0.2949 fb	0.4853 fb	0.5200 fb
$pp \to \tau\tau$ leptonic	10.22 fb	16.18 fb	17.33 fb
$pp \to WW \to \mu\nu_\mu e\nu_e$	2.108 fb	3.682 fb	3.967 fb

Table 4.3: This table shows the leptonic background cross sections for the $\phi \to \tau\mu$ signal with $M_H = 125.1$ GeV. Here we have already applied our selection rules for the signal that will be further discusses in Section 4.5.

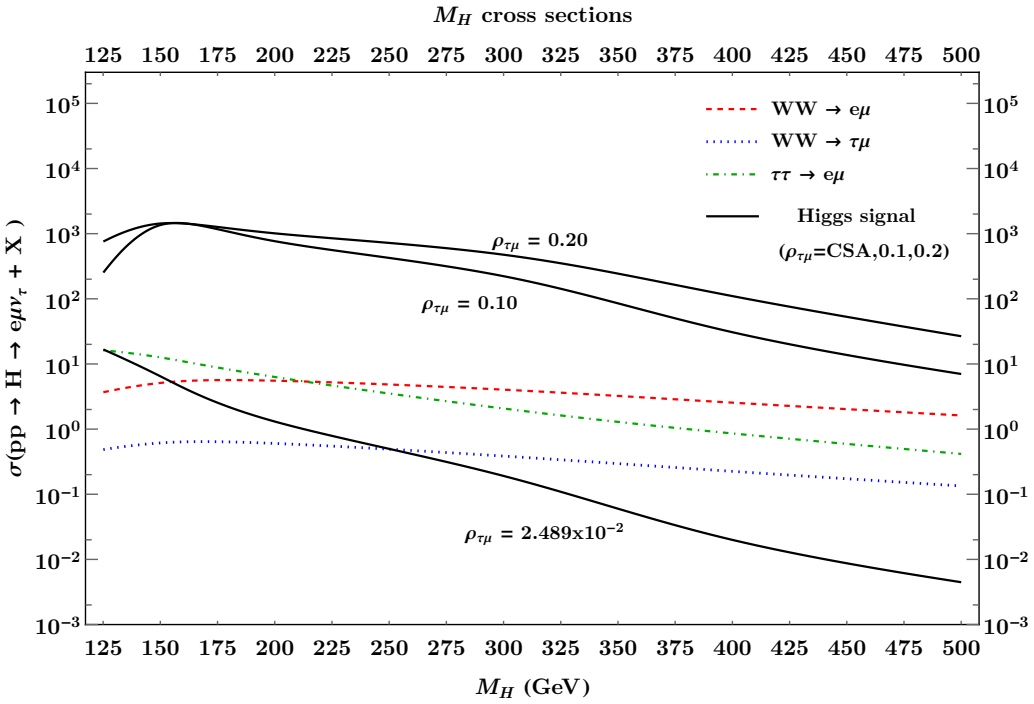

Figure 4.3: Here the SM background for the leptonic decay process at $\sqrt{s} = 13$ TeV is shown as it compares to the signal cross section after full selection cuts. The black curves show the cross section as a function of $M_H \in [125, 500]$ GeV for the various case studies of $\rho_{\tau\mu}$ that were selected: 2.489×10^{-2}, 0.10, 0.20; for $\rho_{tc} = \cos(\beta - \alpha) = 0.1$.

4.4.3 $\phi \to XX$ backgrounds

In both the hadronic decays and the leptonic decays we have another layer of complexity added to our system due to the kinematic regime we are working in. Specifically we have additional backgrounds that, like out signal, are mediated by the SM Higgs paricle. The SM Higgs can decay into a WW^*, a ZZ^*, and a $\tau^+\tau^-$ as well as to the $\tau\mu$ signal we are searching for. Our advantage is, however, that the rate at which it produces these additional particles is much lower than other modes that do not produce the same final state particles we are interested in. The disadvantage that we must overcome is that selecting events based on their ability to reconstruct a Higgs resonance may not be as fruitful for these stats as they do involve a Higgs resonance. Below, Table **4.4**, shows calculated values of these Higgs mediated backgrounds.

$\sigma(pp \to X)$	$\sqrt{s} = 8$ TeV	$\sqrt{s} = 13$ TeV	$\sqrt{s} = 14$ TeV
$pp \to h^0 \to \tau\tau$ leptonic	0.4633 fb	1.004 fb	1.123 fb
$pp \to h^0 \to \tau\tau$ hadronic	2.117 fb	4.581 fb	5.127 fb
$pp \to h^0 \to WW \to \mu\nu_\mu e\nu_e$	4.049×10^{-2} fb	8.881×10^{-2} fb	9.810×10^{-2} fb

Table 4.4: This table shows Higgs mediated background cross sections for the $\phi \to \tau\mu$ signal with $M_H = 125.1$ GeV. Here we have already applied our selection rules for the signal that will be further discusses in Section 4.5.

4.5 Event selection

The background cross sections depicted in Tables **4.2** to **4.4** were all calculated using carefully developed selection rules that were designed to disfavor the background and favor the signal. In any search for an exotic decay mode the best efficiency is obtained by doing your best to exploit the unique physics associated with your signal. In our case, one of the most telling selection rules is the transverse

energy distribution of the final state particles. On this same note, this work has based many of our cuts on the original CMS and ATLAS publications [30, 52], where they apply additional cuts on the angular distibution of the final decay products to isolate the unique properties of the signal. Some of the more novel cuts that were applied in particular to this study are described in more detail below.

4.5.1 Reconstructing the Higgs

Looking at the process $pp \to \phi \to \tau\mu$, another key identifying feature is the presence of a Higgs resonance to generate the $\tau\mu$ final state. To verify that the event we are looking at is indeed our signal this reconstruction must be checked and can also be used to try and discriminate against background processes. As described in Section 4.3, our first step is to correctly and fully reconstruct the tau particle using the collinear approximation. For the signal this allows us to more accurately characterize the central resonance and verify that is was a Higgs. For the background it instead purposefully mischracterizes one of the decay products and will not reconstruct a signal as clean as the $\phi \to \tau\mu$ signal.

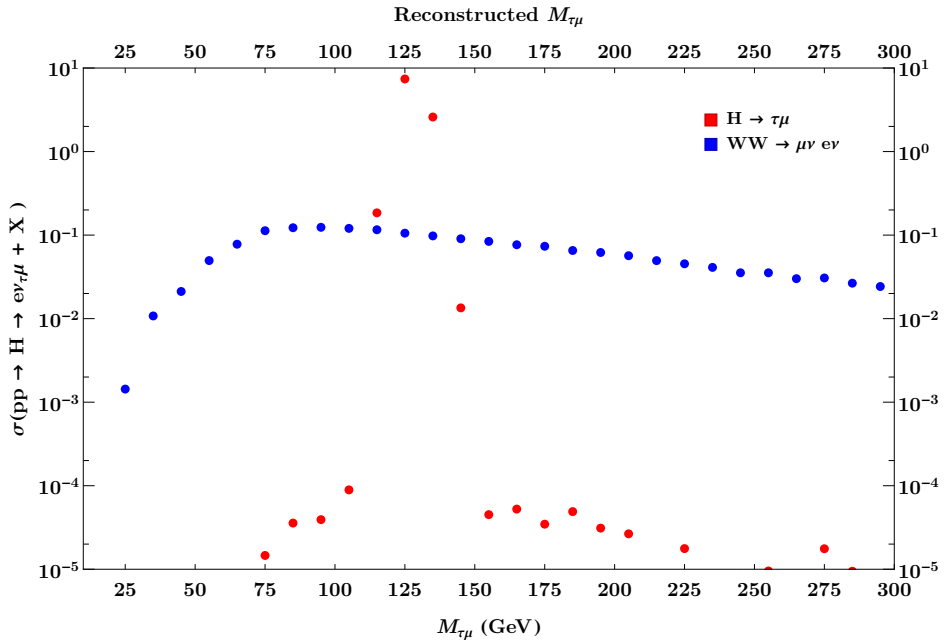

Figure 4.4: This plot shows the reconstructed $\tau\mu$ resonance for our signal and the leptonic WW background. Here it can be seen that the Higgs signal has a sharp peak right at the Higgs mass as expected and the WW process has a much broader shape with a peak much closer to the mass of its dominant resonance, the Z. The above values are shown for a $\sqrt{s} = 8$ TeV and with only basic cuts applied ($p_T > 10$ GeV and $|\eta| < 2.5$).

This mismatch between the shapes and locations of the peaks is what is exploited with such a cut on the reconstructed invariant mass, M_{inv}, of the $\tau\mu$ resonance. It can be somewhat less significant for the $\phi \to XX$ backgrounds but is invaluable for the other electroweak backgrounds.

4.5.2 Importance of transverse mass

As mentioned before, many of our cuts and selection rules are based on information or restrictions imposed by the experimental collaborations, such as p_T and $|\eta|$ requirements for triggers and separation requirements to satisfy isolation cuts in a very naive way. There are some cuts that are also theoretically motivated and can help the experimentalists select data more efficiently. One such

cut for us is a cut on the transverse mass, M_T. Since the tau decay will involve the creation of a neutrino we can expect to have some missing transverse energy in our final state particles.

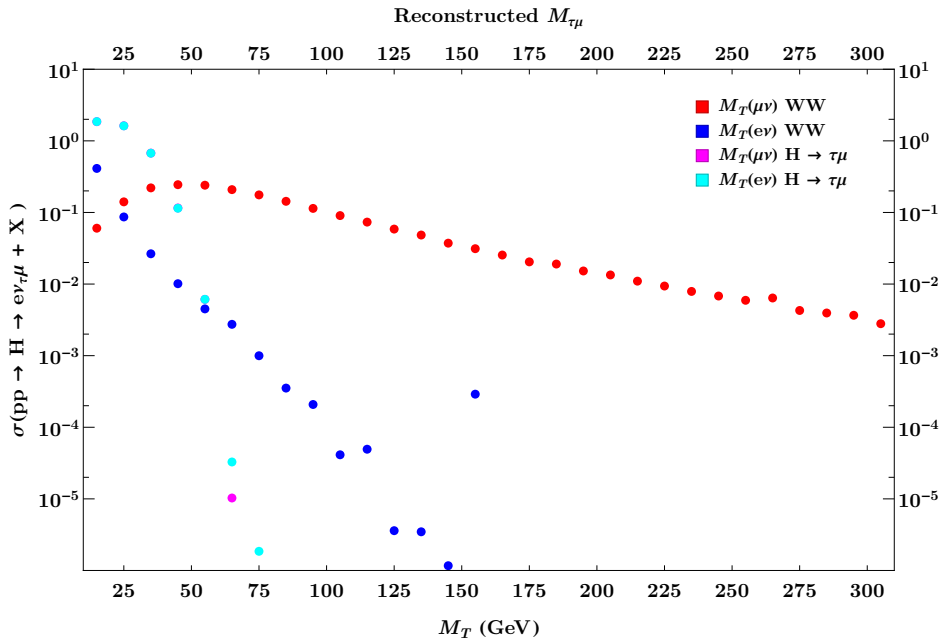

Figure 4.5: This plot shows the transverse mass of the $\mu + \not{E}_T$ and $e + \not{E}_T$ for our signal and the leptonic WW background. Here it can be seen that the WW has symmetric final state partiles whle the signal is more asymmetric. This plot shows the reconstructed $\tau\mu$ resonance for our signal and the leptonic WW background. Here it can be seen that the Higgs signal has a sharp peak right at the Higgs mass as expected and the WW process has a much broader shape with a peak much closer to the mass of its dominant resonance, the Z. The above values are shown for a $\sqrt{s} = 8$ TeV and with only basic cuts applied ($p_T > 10$ GeV and $|\eta| < 2.5$).

We can construct a picture of the transverse mass of a particle, q, in the final state through looking at its transverse components,

$$M_T^2 = \left(p_T(q) + \not{E}_T\right)^2 - \left(q_x + \not{E}_x\right)^2 - \left(q_y + \not{E}_y\right)^2 \qquad (\mathbf{4.6})$$

We can use this to our advantage by applying cuts on the transverse mass of certain particles. Following the lead of CMS, we specifically chose to cut on the transverse mass of a $\mu\nu$ pair and the transverse mass of an $e\nu$ pair. If the final

state particle, say the muon, came from a single particle decay we can expect the transverse mass of that particle have a sharp drop around the mass of the parent particle [53]. Our signal, on the other hand, should exhibit this behavior only in the electron transverse mass and not the muon.

4.5.3 Asymmetric selection rules

Due to the nature all but the $WW \to \tau\mu$ background the processes, we would expect their decays to be symmetric. This is a property that is not shared in the $\phi \to \tau\mu$ signal. Before the tau decays, the two particles are symmetric and, in fact, their momenta are nearly on top of each other as seen in, Figure **4.6**.

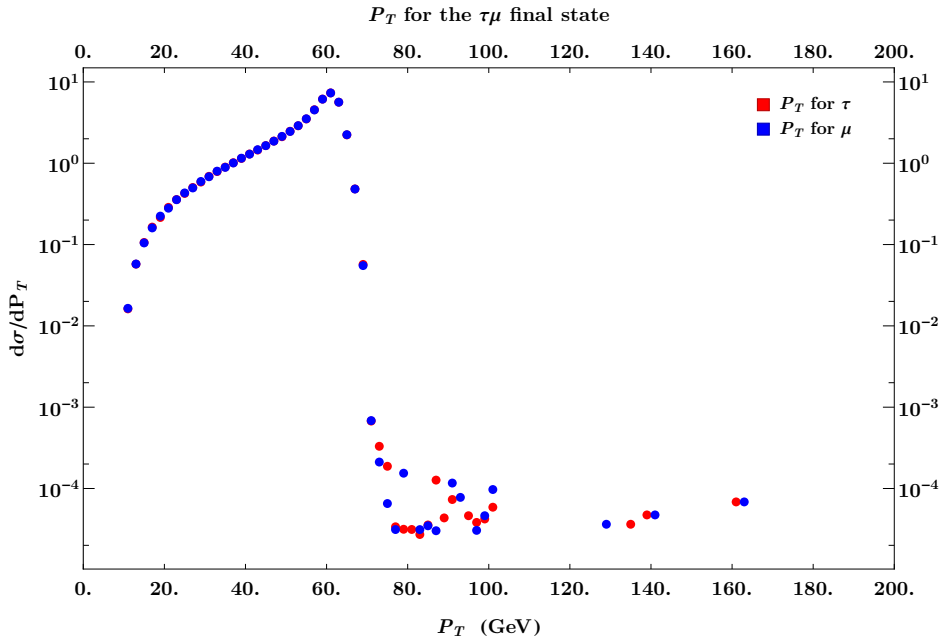

Figure 4.6: Here the p_T for the τ and μ are plotted before any selection cuts are applied. This signature is similar to what is seen in many of the background distributions.

However, once the tau decays into either a jet or a lepton, there is additional energy lost in the form of a neutrinos that will offset the transverse spectrum of the visible particles. Based on this property we have applied some interesting

asymmetric cuts on the P_T and η of the muon and jet or e from the tau decay as highlighted in the table below, Table **4.5**.

Cut Parameter	Leptonic: $\tau \to e\nu_e\nu_\tau$	Hadronic: $\tau \to j\nu_\tau$
$p_T(\mu)$	> 50 GeV	> 45 GeV
$p_T(\tau)$	> 10 GeV	> 35 GeV
$M_T(\mu)$	> 40 GeV	-
$M_T(\tau)$	< 65 GeV	< 50 GeV
$\Delta\phi_{p_T^\mu - p_T^\tau}$	> 2.7	> 2.7
$\Delta\phi_{p_T^\tau - \not{E}_T}$	< 0.5	-
$\lvert\eta_\tau\rvert$	< 2.3	< 2.3
$\lvert\eta_\mu\rvert$	< 2.1	< 2.1

Table 4.5: This table summarizes the cuts applied to the final state particles under the conditions were the tau decays hadronically and is tagged as a jet and when it decays leptonically into an electron. The η cut depicted above is not asymmetric due to the nature of the decay but is chosen to match the trigger efficiency of CMS.

4.6 Results and predictions

Currently, for this study, we look at both the heavy Higgs decay process and the SM-like light Higgs decay as possible signatures for the $\tau\mu$ flavor changing process. All cuts have been applied and cross sections are calculated for heavy Higgs masses from 150 GeV to 500 GeV for $\sqrt{s} = 8,\ 13,\ 14$ TeV using the newly updated CT14 PDFs [1]. For the signal, $M_\phi/2$ is used as the factorization and renormalization scale and the dynamic choice of $\sqrt{s}$ is chosen for all the background processes since they lack a defined core resonance and are mediated, generally, by a γ or a Z. In the case of the Z mediated decays we could adopt a similar factorization scale and renormalization scale to that used for the Higgs signal but such a choice would not

be appropriate for the γ mediated process. All background events are calculated using the same fortran code package developed for the signal process with the exception of importing MG5 matrix elements in lieu of full analytic calculations. For SM processes, MG5 is well tested and used as a benchmark comparison for any study we do to as high a level as we can trust the comparison and only breaks down in the exotic regime or, in the case of H^0, when the effective theory breaks down. But, for well known and tested processes, the use of MG5 matrix elements offers an extra level of confidence in our calculation and the ability to run full detector simulations on the background predictions. The following results were obtained for both leptonic and hadronic tau decay states to be compared against the background cross sections presented in Tables **4.2** to **4.4**.

M_H	125 GeV	150 GeV	200 GeV	300 GeV	400 GeV	500 GeV
top Loop K-factor	1.89743	1.90633	1.92299	1.9447	1.91845	1.87137
bottom loop K-fator	1.04143	1.06498	1.10215	1.15453	1.19169	1.22052
Γ_H GeV $\rho_{\tau\mu} = 0.2$	5.950×10^{-3}	2.410×10^{-1}	3.350×10^{-1}	7.625×10^{-1}	4.662	1.229×10^{1}
Γ_H GeV $\rho_{\tau\mu} = 0.1$	4.146×10^{-3}	6.377×10^{-2}	1.167×10^{-1}	4.080×10^{-1}	4.189	1.170×10^{1}
Γ_H GeV $\rho_{\tau\mu} = 2.489 \times 10^{-2}$	4.176×10^{-3}	8.361×10^{-3}	4.284×10^{-2}	2.972×10^{-1}	4.041	1.151×10^{1}
σ_H (fb) $\rho_{\tau\mu} = 0.2$	5.428	6.380×10^{2}	4.202×10^{2}	1.750×10^{2}	3.742×10^{1}	8.919
σ_H (fb) $\rho_{\tau\mu} = 0.1$	7.790	6.040×10^{2}	3.184×10^{2}	8.190×10^{1}	1.044×10^{1}	2.238
σ_H (fb) $\rho_{\tau\mu} = 2.489 \times 10^{-2}$	7.725	2.883	5.428×10^{-1}	7.036×10^{-2}	6.773×10^{-3}	1.424×10^{-3}

Table 4.6: Cross section data calculated for $h^0/H^0 \to \tau\mu \to \mu e + \not{E}_T + X$ for $\sqrt{s} = 8$ TeV. In all cases the full suite of selection rules have been applied and the total width of each Higgs resonance is reported as calculated using 2HDMC with $\rho_{tc} = \cos(\beta - \alpha) = 0.1$ and $\rho_{\tau\mu}$ as indicated.

M_H	125 GeV	150 GeV	200 GeV	300 GeV	400 GeV	500 GeV
top Loop K-factor	1.89743	1.90633	1.92299	1.9447	1.91845	1.87137
bottom loop K-fator	1.04143	1.06498	1.10215	1.15453	1.19169	1.22052
Γ_H GeV $\rho_{\tau\mu} = 0.2$	5.950×10^{-3}	2.410×10^{-1}	3.350×10^{-1}	7.625×10^{-1}	4.662	1.229×10^{1}
Γ_H GeV $\rho_{\tau\mu} = 0.1$	4.146×10^{-3}	6.377×10^{-2}	1.167×10^{-1}	4.080×10^{-1}	4.189	1.170×10^{1}
Γ_H GeV $\rho_{\tau\mu} = 2.489 \times 10^{-2}$	4.176×10^{-3}	8.361×10^{-3}	4.284×10^{-2}	2.972×10^{-1}	4.041	1.151×10^{1}
σ_H (fb) $\rho_{\tau\mu} = 0.2$	1.173×10^{1}	1.426×10^{3}	9.992×10^{2}	4.642×10^{2}	1.097×10^{2}	2.740×10^{1}
σ_H (fb) $\rho_{\tau\mu} = 0.1$	1.566×10^{1}	1.350×10^{3}	7.571×10^{2}	2.172×10^{2}	3.061×10^{1}	7.210
σ_H (fb) $\rho_{\tau\mu} = 2.489 \times 10^{-2}$	1.669×10^{1}	6.446	1.291	1.866×10^{-1s}	1.986×10^{-2}	4.587×10^{-3}

Table 4.7: Cross section data calculated for $h^0/H^0 \to \tau\mu \to \mu e + \not{E}_T + X$ for $\sqrt{s} = 13$ TeV. In all cases the full suite of selection rules have been applied and the total width of each Higgs resonance is reported as calculated using 2HDMC with $\rho_{tc} = \cos(\beta - \alpha) = 0.1$ and $\rho_{\tau\mu}$ as indicated.

M_H	125 GeV	150 GeV	200 GeV	300 GeV	400 GeV	500 GeV
top Loop K-factor	1.89743	1.90633	1.92299	1.9447	1.91845	1.87137
bottom loop K-fator	1.04143	1.06498	1.10215	1.15453	1.19169	1.22052
Γ_H GeV $\rho_{\tau\mu} = 0.2$	5.950×10^{-3}	2.410×10^{-1}	3.350×10^{-1}	7.625×10^{-1}	4.662	1.229×10^{1}
Γ_H GeV $\rho_{\tau\mu} = 0.1$	4.146×10^{-3}	6.377×10^{-2}	1.167×10^{-1}	4.080×10^{-1}	4.189	1.170×10^{1}
Γ_H GeV $\rho_{\tau\mu} = 2.489 \times 10^{-2}$	4.176×10^{-3}	8.361×10^{-3}	4.284×10^{-2}	2.972×10^{-1}	4.041	1.151×10^{1}
σ_H (fb) $\rho_{\tau\mu} = 0.2$	1.311×10^{1}	1.602×10^{3}	1.132×10^{3}	5.332×10^{2}	1.276×10^{2}	3.224×10^{1}
σ_H (fb) $\rho_{\tau\mu} = 0.1$	1.751×10^{1}	1.517×10^{3}	8.576×10^{2}	2.495×10^{2}	3.560×10^{1}	8.483
σ_H (fb) $\rho_{\tau\mu} = 2.489 \times 10^{-2}$	1.867×10^{1}	7.242	1.462	2.144×10^{-2}	2.310×10^{-2}	5.397×10^{-3}

Table 4.8: Cross section data calculated for $h^0/H^0 \to \tau\mu \to \mu e + \not{E}_T + X$ for $\sqrt{s} = 14$ TeV. In all cases the full suite of selection rules have been applied and the total width of each Higgs resonance is reported as calculated using 2HDMC with $\rho_{tc} = \cos(\beta - \alpha) = 0.1$ and $\rho_{\tau\mu}$ as indicated.

M_H	125 GeV	150 GeV	200 GeV	300 GeV	400 GeV	500 GeV
top Loop K-factor	1.89743	1.90633	1.92299	1.9447	1.91845	1.87137
bottom loop K-fator	1.04143	1.06498	1.10215	1.15453	1.19169	1.22052
Γ_H GeV $\rho_{\tau\mu} = 0.2$	5.950×10^{-3}	2.410×10^{-1}	3.350×10^{-1}	7.625×10^{-1}	4.662	1.229×10^{1}
Γ_H GeV $\rho_{\tau\mu} = 0.1$	4.146×10^{-3}	6.377×10^{-2}	1.167×10^{-1}	4.080×10^{-1}	4.189	1.170×10^{1}
Γ_H GeV $\rho_{\tau\mu} = 2.489 \times 10^{-2}$	4.176×10^{-3}	8.361×10^{-3}	4.284×10^{-2}	2.972×10^{-1}	4.041	1.151×10^{1}
σ_H (fb) $\rho_{\tau\mu} = 0.2$	1.486×10^{1}	1.820×10^{3}	1.255×10^{3}	5.401×10^{2}	1.168×10^{2}	2.649×10^{1}
σ_H (fb) $\rho_{\tau\mu} = 0.1$	1.984×10^{1}	1.723×10^{3}	9.511×10^{2}	2.528×10^{2}	3.259×10^{1}	6.972
σ_H (fb) $\rho_{\tau\mu} = 2.489 \times 10^{-2}$	2.114×10^{1}	8.227	1.622	2.172×10^{-1}	2.115×10^{-2}	4.436×10^{-3}

Table 4.9: Cross section data calculated for $h^0/H^0 \to \tau\mu \to \mu j_\tau + \not{E}_T + X$ for $\sqrt{s} = 8$ TeV. In all cases the full suite of selection rules have been applied and the total width of each Higgs resonance is reported as calculated using 2HDMC with $\rho_{tc} = \cos(\beta - \alpha) = 0.1$ and $\rho_{\tau\mu}$ as indicated.

M_H	125 GeV	150 GeV	200 GeV	300 GeV	400 GeV	500 GeV
top Loop K-factor	1.89743	1.90633	1.92299	1.9447	1.91845	1.87137
bottom loop K-fator	1.04143	1.06498	1.10215	1.15453	1.19169	1.22052
Γ_H GeV $\rho_{\tau\mu} = 0.2$	5.950×10^{-3}	2.410×10^{-1}	3.350×10^{-1}	7.625×10^{-1}	4.662	1.229×10^{1}
Γ_H GeV $\rho_{\tau\mu} = 0.1$	4.146×10^{-3}	6.377×10^{-2}	1.167×10^{-1}	4.080×10^{-1}	4.189	1.170×10^{1}
Γ_H GeV $\rho_{\tau\mu} = 2.489 \times 10^{-2}$	4.176×10^{-3}	8.361×10^{-3}	4.284×10^{-2}	2.972×10^{-1}	4.041	1.151×10^{1}
σ_H (fb) $\rho_{\tau\mu} = 0.2$	3.209×10^{1}	4.070×10^{3}	2.986×10^{3}	1.434×10^{3}	3.429×10^{2}	8.540×10^{1}
σ_H (fb) $\rho_{\tau\mu} = 0.1$	4.284×10^{1}	3.853×10^{3}	2.263×10^{3}	6.710×10^{2}	9.564×10^{1}	2.247×10^{1}
σ_H (fb) $\rho_{\tau\mu} = 2.489 \times 10^{-2}$	4.565×10^{1}	1.839×10^{1}	3.858	5.764×10^{-1}	6.206×10^{-2}	1.430×10^{-2}

Table 4.10: Cross section data calculated for $h^0/H^0 \to \tau\mu \to \mu j_\tau + \not{E}_T + X$ for $\sqrt{s} = 13$ TeV. In all cases the full suite of selection rules have been applied and the total width of each Higgs resonance is reported as calculated using 2HDMC with $\rho_{tc} = \cos(\beta - \alpha) = 0.1$ and $\rho_{\tau\mu}$ as indicated.

M_H	125 GeV	150 GeV	200 GeV	300 GeV	400 GeV	500 GeV
top Loop K-factor	1.89743	1.90633	1.92299	1.9447	1.91845	1.87137
bottom loop K-fator	1.04143	1.06498	1.10215	1.15453	1.19169	1.22052
Γ_H GeV $\rho_{\tau\mu} = 0.2$	5.950×10^{-3}	2.410×10^{-1}	3.350×10^{-1}	7.625×10^{-1}	4.662	1.229×10^{1}
Γ_H GeV $\rho_{\tau\mu} = 0.1$	4.146×10^{-3}	6.377×10^{-2}	1.167×10^{-1}	4.080×10^{-1}	4.189	1.170×10^{1}
Γ_H GeV $\rho_{\tau\mu} = 2.489 \times 10^{-2}$	4.176×10^{-3}	8.361×10^{-3}	4.284×10^{-2}	2.972×10^{-1}	4.041	1.151×10^{1}
σ_H (fb) $\rho_{\tau\mu} = 0.2$	3.588×10^{1}	4.573×10^{3}	3.383×10^{3}	1.647×10^{3}	3.988×10^{2}	3.224×10^{1}
σ_H (fb) $\rho_{\tau\mu} = 0.1$	4.790×10^{1}	4.329×10^{3}	2.563×10^{3}	7.708×10^{2}	1.112×10^{1}	2.644×10^{1}
σ_H (fb) $\rho_{\tau\mu} = 2.489 \times 10^{-2}$	5.105×10^{1}	2.067×10^{1}	4.370	6.622×10^{-1}	7.219×10^{-2}	1.682×10^{-3}

Table 4.11: Cross section data calculated for $h^0/H^0 \to \tau\mu \to \mu j_\tau + \not{E}_T + X$ for $\sqrt{s} = 14$ TeV. In all cases the full suite of selection rules have been applied and the total width of each Higgs resonance is reported as calculated using 2HDMC with $\rho_{tc} = \cos(\beta - \alpha) = 0.1$ and $\rho_{\tau\mu}$ as indicated.

The work for this project is ongoing, as we still need to look at the pseudoscalar signal and extend the mass range for the Heavy Higgs process out to ≈ 1 TeV as was done with the htc project. The final results will then be submitted for publication. With the additional data and further refinement of the search, namely in the context of more points and a higher fidelity scan as a function of Higgs mass, discovery potentials will be created to visually represent our findings. Preliminary findings suggest that the end of Run II should provide us with enough data to have seen enough evidence of a $\tau\mu$ flavor changing process involving a light, SM-like Higgs boson with a coupling as low as our base value of $\rho_{\tau\mu} = 2.489 \times 10^{-2}$ while we will need at least 1800 fb^{-1} before we can see such a signal in the heavy Higgs sector making such a signal not visible until after the high luminosity upgrade of the LHC.

Chapter 5

Conclusion: A Look Beyond the Standard Model

> "*The most beautiful thing we can experience is the mysterious. It is the source of all true art and science.*"
>
> — Albert Einstein, *What I believe*

Science, by nature, is the attempt to understand the world around you and be able to make predictions on how nature will behave. Earlier I mentioned how Newtonian Mechanics is to Relativity as the Standard Model is to Beyond the Standard Model and so it is only appropriate that what began with a quote from Newton is summed up by a quote from Einstein. In both cases, I must agree whole heartedly with their statements. Particle physics is not unique in going beyond the standard physics of everyday life and looking at something deeper but I do find it unique in how well defined and documented its history is. What we learn from papers now will be written down in books before too long and a lot of that has to do with how the field handles itself and propagates its own wavefunction forward in time. And so it is with this work.

Though our goals were not as lofty as grand unified theories, or even full extensions and replacements of the SM, our work does serve an important role in describing and predicting what may be seen in a corner of particle physics. The Higgs sector, as the newest sector to be discovered experimentally, still has much to provide us with in terms of information in how the Yukawa couplings work and why some particles are so much more massive than the other. Our research also shows, that it is possible and likely that this is one of the areas in which we will first see evidence of new physics. new physics, we define as physics beyond the SM. As Run II is wrapping up we hope some of the data may either match

our predictions for flavor changing neutral currents or help further constrain the parameter space for future dedicated studies. Both the leptonic, $\tau\mu$, and the hadronic, tc, flavor changing interactions still have a fairly large parameter space in which the couplings might lie and the more we find out about this parameter space the more we will know about the alignment limit, $\cos(\beta - \alpha)$, and the diagonal mass-based Yukawa couplings that are stored in the κ and ρ matrices.

We acknowledge that it is also possible the general treatment of the Two Higgs Doublet Model is too generous and needs to be further constrained as in the Type-II model required by SUSY but we have no direct indications of that yet. We hope this study will help us gain some more insight. We will be finishing up the $\tau\mu$ project soon after refining some of the data with higher fidelity information that we were not able to collect until now and studies into the ρ_{tc} coupling will continue in the group going forward as there is a lot that can be done with the kenematically viable $t \to ch^0$ decay mode. Some preliminary work has already been completed and will, hopefully, be finished by the end of the calendar year.

Flavor changing neutral currents mediated by Higgs bosons are not the answer to all the questions the SM needs some help resolving, but they are a small step in a direction that can tell us a lot about how nature works. And to anyone who says particle physics is dead and there isn't anything left to find I simply say, look harder, the answers are there, we just need to find them.

References

[1] T.-J. Hou *et al.*, Phys. Rev. **D95**, 034003 (2017), arXiv:1609.07968.

[2] A. D. Martin, W. J. Stirling, R. S. Thorne, and G. Watt, Eur. Phys. J. **C63**, 189 (2009), arXiv:0901.0002.

[3] ATLAS, G. Aad *et al.*, Phys. Lett. **B716**, 1 (2012), arXiv:1207.7214.

[4] CMS, S. Chatrchyan *et al.*, Phys. Lett. **B716**, 30 (2012), arXiv:1207.7235.

[5] K. A. Milton, editor, *A quantum legacy: Seminal papers of Julian Schwinger* (, 2000).

[6] R. P. Feynman, World Sci. Ser.20th Cent. Phys. **27**, pp.1 (2000).

[7] S.-I. Tomonaga, Development of Quantum Electrodynamics, in *The Physicist's Conception of Nature*, pp. 404–412, Springer Netherlands, Dordrecht, 1966.

[8] F. J. Dyson, *Selected papers of Freeman Dyson with commentary* (, 1996).

[9] C.-N. Yang and R. L. Mills, Phys. Rev. **96**, 191 (1954).

[10] G. C. Branco, L. Lavoura, and J. P. Silva, Int. Ser. Monogr. Phys. **103**, 1 (1999).

[11] M. H. Seymour, Quantum chromodynamics, in *2004 European School of High-Energy Physics, Sant Feliu de Guixols, Spain, 30 May - 12 June 2004*, pp. 49–94, 2005, arXiv:hep-ph/0505192.

[12] G. 't Hooft, Spontaneous breakdown of local conformal invariance in quantum gravity, in *Lecture Notes, Les Houches Summer School, 97th Session: Theoretical Physics to Face the Challenge of LHC: Les Houches, France, August 1-26, 2011*, pp. 209–250, 2015.

[13] S. Van Den Bergh, (2000), arXiv:0005314v1.

[14] B. Pontecorvo, (1957).

[15] I. I. Y. Bigi and A. I. Sanda, Camb. Monogr. Part. Phys. Nucl. Phys. Cosmol. **9**, 1 (2000).

[16] V. Elias and T. N. Sherry, (1980).

[17] H. Baer and X. Tata, *Weak scale supersymmetry: From superfields to scattering events* (Cambridge University Press, 2006 and references therein).

[18] A. Linde, Rept. Prog. Phys. **80**, 022001 (2017), arXiv:1512.01203.

[19] J. H. Schwarz, NATO Sci. Ser. C **566**, 143 (2001), arXiv:hep-ex/0008017.

[20] T. Ibrahim and P. Nath, Rev. Mod. Phys. **80**, 577 (2008), arXiv:0705.2008.

[21] R. D. Peccei and H. R. Quinn, Phys. Rev. Lett. **38**, 1440 (1977).

[22] J. F. Gunion, H. E. Haber, G. L. Kane, and S. Dawson, Front. Phys. **80**, 1 (2000 and references therein).

[23] Particle Data Group, C. Patrignani *et al.*, Chin. Phys. **C40**, 100001 (2016).

[24] G. C. Branco *et al.*, Theory and phenomenology of two-Higgs-doublet models, 2012, arXiv:1106.0034.

[25] J. F. Gunion and H. E. Haber, Phys. Rev. **D67**, 075019 (2003), arXiv:hep-ph/0207010.

[26] F. Mahmoudi and O. Stal, Phys. Rev. **D81**, 035016 (2010), arXiv:0907.1791.

[27] S. L. Glashow, J. Iliopoulos, and L. Maiani, Phys. Rev. **D2**, 1285 (1970).

[28] N. Craig, J. Galloway, and S. Thomas, (2013), arXiv:1305.2424.

[29] M. Carena, I. Low, N. R. Shah, and C. E. M. Wagner, JHEP **04**, 015 (2014), arXiv:1310.2248.

[30] CMS, V. Khachatryan *et al.*, Phys. Lett. **B749**, 337 (2015), arXiv:1502.07400.

[31] M. E. Peskin and D. V. Schroeder, *An Introduction to quantum field theory* (Addison-Wesley, Reading, USA, 1995).

[32] J. Brehmer, A. Freitas, D. Lopez-Val, and T. Plehn, Phys. Rev. **D93**, 075014 (2016), arXiv:1510.03443.

[33] G. Passarino and M. J. G. Veltman, Nucl. Phys. **B160**, 151 (1979).

[34] J. Alwall *et al.*, JHEP **07**, 079 (2014), arXiv:1405.0301.

[35] CMS, C. Collaboration, (2016).

[36] CMS, C. Collaboration, (2015).

[37] ATLAS, M. Aaboud *et al.*, JHEP **09**, 001 (2016), arXiv:1606.03833.

[38] CERN Report No. ATLAS-CONF-2015-081, 2015 (unpublished).

[39] C. Campagnari and M. Franklin, Rev. Mod. Phys. **69**, 137 (1997), arXiv:hep-ex/9608003.

[40] B. Altunkaynak, W.-S. Hou, C. Kao, M. Kohda, and B. McCoy, Phys. Lett. **B751**, 135 (2015), arXiv:1506.00651.

[41] G. Bhattacharyya, D. Das, and A. Kundu, Phys. Rev. **D89**, 095029 (2014), arXiv:1402.0364.

[42] *The CKM matrix and the unitarity triangle. Workshop, CERN, Geneva, Switzerland, 13-16 Feb 2002: Proceedings*, 2003, arXiv:hep-ph/0304132.

[43] N. Cabibbo, Phys. Rev. Lett. **10**, 531 (1963), [,648(1963)].

[44] ATLAS, G. Aad *et al.*, (2009), arXiv:0901.0512.

[45] CMS, G. L. Bayatian *et al.*, J. Phys. **G34**, 995 (2007).

[46] ATLAS Collaboration, P. Jenni, M. Nessi, M. Nordberg, and K. Smith, *ATLAS high-level trigger, data-acquisition and controls: Technical Design Report*Technical Design Report ATLAS (CERN, Geneva, 2003).

[47] CERN Report No. ATL-PHYS-PUB-2013-012, 2013 (unpublished).

[48] G. Apollinari, O. Brüning, T. Nakamoto, and L. Rossi, CERN Yellow Report , 1 (2015), arXiv:1705.08830.

[49] BaBar, B. Aubert *et al.*, Phys. Rev. Lett. **104**, 021802 (2010), arXiv:0908.2381.

[50] T. Aushev *et al.*, (2010), arXiv:1002.5012.

[51] K. Hagiwara, A. D. Martin, and D. Zeppenfeld, Phys. Lett. **B235**, 198 (1990).

[52] ATLAS, G. Aad *et al.*, Eur. Phys. J. **C77**, 70 (2017), arXiv:1604.07730.

[53] CMS, V. Khachatryan *et al.*, JHEP **03**, 032 (2017), arXiv:1606.01522.

[54] M. Spira, (1995), arXiv:hep-ph/9510347.

[55] D. Eriksson, J. Rathsman, and O. Stal, Comput. Phys. Commun. **181**, 189 (2010), arXiv:0902.0851.

[56] R. Boughezal *et al.*, Eur. Phys. J. **C77**, 7 (2017), arXiv:1605.08011.

[57] A. Alloul, N. D. Christensen, C. Degrande, C. Duhr, and B. Fuks, Comput. Phys. Commun. **185**, 2250 (2014), arXiv:1310.1921.

Important Programs

In order to perform crucial calculations and predict what we may see we have to develop our own code and methods of both creating and analyzing the data we need in order to make reliable predictions some of the tools we use are:

- **MadGraph** [34]: a software sweet that allows us to run detector simulations on physical decay processes involving most common models with features that allow for the import of your own models.

- **ROOT**: a data analysis framework developed and maintained by CERN that allow us to analyze data and the detector simulations produced by MadGraph in ways similar to the experimentalists.

- **HIGLU** [54]: a piece of software specifically designed to numerically evaluate leading order (LO), next to leading order (NLO), and even next-to-next-to leading order (NNLO) $gg \to \phi^0$ production so we can calculate appropriate K-factors.

- **2HDMC** [55]: software designed to analyze Higgs decays under several different BSM models, including the 2HDM. This software allows us to calculate total width and branching ratio information for Higgs bosons under a broad phase-space region.

- **MCFM** [56]: software developed at Fermilab to calculate LO, NLO, and NNLO information for several common SM processes such as WW or $t\bar{t}$ production with various decay modes. This software is used to calculate k-factors for many of our background processes.

- **VEGAS**: is a linux/unix based numerical integration routine that utilizes important sampling to map out abrupt features of your decay processes so

that we can produce realistic collider data for analysis.

- **FeynRules** [57]: a Mathematica package used to create model files to use with MadGraph that includes the ability to do process level coupling verification and will check itself for invariance and Hermiticity.

- **FORM**: software developed to calculate traces like the one shown in Equation (**2.2**) and apply tensor reduction techniques for more reliable simplification.

- **Fortran Code**: self developed Fortran programs and analysis were created and implemented to evaluate the complex integrals involved in cross section calculations, apply necessary selection cuts, construct the kinematics of the process, and generate histogram data for analysis.

Table 1: K-factors calculated from higlu for the production of the light, heavy, and pseudoscalar Higgs bosons through glun-gluon fusion via a heavy quark loop (top and bottom). For the top loop, these are next-to-next-to leading order (NLLO) to leading order (LO) ratios and for the bottom loop they are next-to leading order of LO ratios.

M_H GeV	top loop kFactor (formula)	bottom loop kFactor (formula)
125	1.92443	1.01226
150	1.93552	1.03564
175	1.94828	1.0554
200	1.96019	1.07253
225	1.9708	1.08763
250	1.98166	1.10114
275	1.99637	1.11336
300	2.02058	1.12451
325	2.06195	1.13478
350	2.13018	1.14428
375	1.94282	1.15313
400	1.90573	1.1614
425	1.88406	1.16918
450	1.8687	1.1765
475	1.85679	1.18344
500	1.84705	1.19001
525	1.83883	1.19627
550	1.8317	1.20223
575	1.82542	1.20793
600	1.81979	1.21339
625	1.81471	1.21863
650	1.81007	1.22365
675	1.8058	1.22849
700	1.80184	1.23316
725	1.79816	1.23766
750	1.79472	1.242
775	1.79148	1.24621
800	1.78844	1.25028
825	1.78555	1.25422
850	1.78282	1.25805
875	1.78021	1.26177
900	1.77773	1.26538
925	1.77536	1.26889
950	1.77309	1.27231
975	1.77091	1.27564
1000	1.76882	1.27889

Additional Data

The other test cases that were studied set $\rho_{tc} = 2.501 \times 10^{-3},\ 0.50$ and $\rho_{\tau\mu} = 2.489 \times 10^{-3},\ 0.20$. Below are data sets for each of those test cases.

M_H	125 GeV	150 GeV	200 GeV	300 GeV	400 GeV	500 GeV
top Loop K-factor	1.89743	1.90633	1.92299	1.9447	1.91845	1.87137
bottom loop K-fator	1.04143	1.06498	1.10215	1.15453	1.19169	1.22052
Γ_H GeV $\rho_{\tau\mu} = 0.2$	5.950×10^{-3}	2.410×10^{-1}	7.860×10^{-1}	5.341	1.367×10^{1}	2.543×10^{1}
Γ_H GeV $\rho_{\tau\mu} = 0.1$	4.146×10^{-3}	6.377×10^{-2}	5.497×10^{-1}	4.987	1.319×10^{1}	2.484×10^{1}
Γ_H GeV $\rho_{\tau\mu} = 2.489 \times 10^{-2}$	4.176×10^{-3}	8.361×10^{-3}	4.758×10^{-1}	4.876	1.305×10^{1}	2.465×10^{1}
σ_H (fb) $\rho_{\tau\mu} = 0.2$	5.428	6.380×10^{2}	1.880×10^{2}	2.445×10^{1}	1.215×10^{1}	3.922
σ_H (fb) $\rho_{\tau\mu} = 0.1$	7.790	6.040×10^{2}	6.734×10^{1}	6.556	3.156	1.006
σ_H (fb) $\rho_{\tau\mu} = 2.489 \times 10^{-2}$	1.867×10^{1}	2.883	4.870×10^{-2}	4.197×10^{-3}	1.997×10^{-3}	6.345×10^{-4}

Table 2: $\sqrt{s} = 8$ TeV Leptonic Decay with $\rho_{tc} = 0.50$

M_H	125 GeV	150 GeV	200 GeV	300 GeV	400 GeV	500 GeV
top Loop K-factor	1.89743	1.90633	1.92299	1.9447	1.91845	1.87137
bottom loop K-fator	1.04143	1.06498	1.10215	1.15453	1.19169	1.22052
Γ_H GeV $\rho_{\tau\mu} = 0.2$	5.950×10^{-3}	2.410×10^{-1}	3.350×10^{-1}	7.625×10^{-1}	4.662	1.229×10^{1}
Γ_H GeV $\rho_{\tau\mu} = 0.1$	4.146×10^{-3}	6.377×10^{-2}	1.167×10^{-1}	4.080×10^{-1}	4.189	1.170×10^{1}
Γ_H GeV $\rho_{\tau\mu} = 2.489 \times 10^{-2}$	4.176×10^{-3}	8.361×10^{-3}	4.758×10^{-1}	4.876	1.305×10^{1}	2.465×10^{1}
σ_H (fb) $\rho_{\tau\mu} = 0.2$	1.173×10^{1}	1.426×10^{3}	4.471×10^{2}	6.487×10^{1}	3.564×10^{1}	1.263×10^{1}
σ_H (fb) $\rho_{\tau\mu} = 0.1$	1.566×10^{1}	1.350×10^{3}	1.601×10^{2}	1.740×10^{1}	9.259	3.239
σ_H (fb) $\rho_{\tau\mu} = 2.489 \times 10^{-2}$	1.669×10^{1}	6.446	1.158×10^{-1}	1.114×10^{-2}	5.858×10^{-3}	2.043×10^{-3}

Table 3: $\sqrt{s} = 13$ TeV Leptonic Decay with $\rho_{tc} = 0.50$

M_H	125 GeV	150 GeV	200 GeV	300 GeV	400 GeV	500 GeV
top Loop K-factor	1.89743	1.90633	1.92299	1.9447	1.91845	1.87137
bottom loop K-fator	1.04143	1.06498	1.10215	1.15453	1.19169	1.22052
Γ_H GeV $\rho_{\tau\mu} = 0.2$	5.950×10^{-3}	2.410×10^{-1}	3.350×10^{-1}	7.625×10^{-1}	4.662	1.229×10^{1}
Γ_H GeV $\rho_{\tau\mu} = 0.1$	4.146×10^{-3}	6.377×10^{-2}	1.167×10^{-1}	4.080×10^{-1}	4.189	1.170×10^{1}
Γ_H GeV $\rho_{\tau\mu} = 2.489 \times 10^{-2}$	4.176×10^{-3}	8.361×10^{-3}	4.758×10^{-1}	4.876	1.305×10^{1}	2.465×10^{1}
σ_H (fb) $\rho_{\tau\mu} = 0.2$	1.311×10^{1}	1.602×10^{3}	5.065×10^{2}	7.452×10^{1}	4.146×10^{1}	1.486×10^{1}
σ_H (fb) $\rho_{\tau\mu} = 0.1$	1.751×10^{1}	1.517×10^{3}	1.814×10^{2}	1.999×10^{1}	1.077×10^{1}	3.811
σ_H (fb) $\rho_{\tau\mu} = 2.489 \times 10^{-2}$	1.867×10^{1}	7.242	1.312×10^{-1}	1.279×10^{-2}	6.814×10^{-3}	2.403×10^{-3}

Table 4: $\sqrt{s} = 14$ TeV Leptonic Decay with $\rho_{tc} = 0.50$

M_H	125 GeV	150 GeV	200 GeV	300 GeV	400 GeV	500 GeV
top Loop K-factor	1.89743	1.90633	1.92299	1.9447	1.91845	1.87137
bottom loop K-fator	1.04143	1.06498	1.10215	1.15453	1.19169	1.22052
Γ_H GeV $\rho_{\tau\mu} = 0.2$	5.950×10^{-3}	2.410×10^{-1}	3.350×10^{-1}	7.625×10^{-1}	4.662	1.229×10^{1}
Γ_H GeV $\rho_{\tau\mu} = 0.1$	4.146×10^{-3}	6.377×10^{-2}	1.167×10^{-1}	4.080×10^{-1}	4.189	1.170×10^{1}
Γ_H GeV $\rho_{\tau\mu} = 2.489 \times 10^{-2}$	4.176×10^{-3}	8.361×10^{-3}	4.758×10^{-1}	4.876	1.305×10^{1}	2.465×10^{1}
σ_H (fb) $\rho_{\tau\mu} = 0.2$	1.486×10^{1}	1.820×10^{3}	5.617×10^{2}	7.545×10^{1}	3.793×10^{1}	8.504
σ_H (fb) $\rho_{\tau\mu} = 0.1$	1.984×10^{1}	1.723×10^{3}	2.012×10^{2}	2.024×10^{1}	9.852	3.134
σ_H (fb) $\rho_{\tau\mu} = 2.489 \times 10^{-2}$	5.105×10^{1}	8.227	1.455×10^{-1}	1.295×10^{-2}	6.234×10^{-3}	1.977×10^{-3}

Table 5: $\sqrt{s} = 8$ TeV Hadronic Decay with $\rho_{tc} = 0.50$

M_H	125 GeV	150 GeV	200 GeV	300 GeV	400 GeV	500 GeV
top Loop K-factor	1.89743	1.90633	1.92299	1.9447	1.91845	1.87137
bottom loop K-fator	1.04143	1.06498	1.10215	1.15453	1.19169	1.22052
Γ_H GeV $\rho_{\tau\mu} = 0.2$	5.950×10^{-3}	2.410×10^{-1}	3.350×10^{-1}	7.625×10^{-1}	4.662	1.229×10^{1}
Γ_H GeV $\rho_{\tau\mu} = 0.1$	4.146×10^{-3}	6.377×10^{-2}	1.167×10^{-1}	4.080×10^{-1}	4.189	1.170×10^{1}
Γ_H GeV $\rho_{\tau\mu} = 2.489 \times 10^{-2}$	4.176×10^{-3}	8.361×10^{-3}	4.758×10^{-1}	4.876	1.305×10^{1}	2.465×10^{1}
σ_H (fb) $\rho_{\tau\mu} = 0.2$	3.209×10^{1}	4.070×10^{3}	1.336×10^{3}	2.004×10^{2}	1.114×10^{2}	3.936×10^{1}
σ_H (fb) $\rho_{\tau\mu} = 0.1$	4.284×10^{1}	3.853×10^{3}	4.786×10^{2}	5.374×10^{1}	2.4893×10^{1}	1.009×10^{1}
σ_H (fb) $\rho_{\tau\mu} = 2.489 \times 10^{-2}$	4.565×10^{1}	1.839×10^{1}	3.461×10^{-1}	3.439×10^{-2}	1.830×10^{-2}	6.367×10^{-3}

Table 6: $\sqrt{s} = 13$ TeV Hadronic Decay with $\rho_{tc} = 0.50$

M_H	125 GeV	150 GeV	200 GeV	300 GeV	400 GeV	500 GeV
top Loop K-factor	1.89743	1.90633	1.92299	1.9447	1.91845	1.87137
bottom loop K-fator	1.04143	1.06498	1.10215	1.15453	1.19169	1.22052
Γ_H GeV $\rho_{\tau\mu} = 0.2$	5.950×10^{-3}	2.410×10^{-1}	3.350×10^{-1}	7.625×10^{-1}	4.662	1.229×10^{1}
Γ_H GeV $\rho_{\tau\mu} = 0.1$	4.146×10^{-3}	6.377×10^{-2}	1.167×10^{-1}	4.080×10^{-1}	4.189	1.170×10^{1}
Γ_H GeV $\rho_{\tau\mu} = 2.489 \times 10^{-2}$	4.176×10^{-3}	8.361×10^{-3}	4.758×10^{-1}	4.876	1.305×10^{1}	2.465×10^{1}
σ_H (fb) $\rho_{\tau\mu} = 0.2$	3.588×10^{1}	4.573×10^{3}	1.514×10^{3}	2.302×10^{2}	1.295×10^{2}	4.631×10^{1}
σ_H (fb) $\rho_{\tau\mu} = 0.1$	4.790×10^{1}	4.329×10^{3}	5.422×10^{2}	6.174×10^{1}	3.365×10^{1}	1.188×10^{1}
σ_H (fb) $\rho_{\tau\mu} = 2.489 \times 10^{-2}$	5.105×10^{1}	2.067×10^{1}	3.921×10^{-1}	3.952×10^{-2}	2.129×10^{-2}	7.492×10^{-3}

Table 7: $\sqrt{s} = 14$ TeV Hadronic Decay with $\rho_{tc} = 0.50$

M_H	125 GeV	150 GeV	200 GeV	300 GeV	400 GeV	500 GeV
top Loop K-factor	1.89743	1.90633	1.92299	1.9447	1.91845	1.87137
bottom loop K-fator	1.04143	1.06498	1.10215	1.15453	1.19169	1.22052
Γ_H GeV $\rho_{\tau\mu} = 0.2$	5.950×10^{-3}	2.410×10^{-1}	3.350×10^{-1}	5.714×10^{-1}	4.286	1.174×10^{1}
Γ_H GeV $\rho_{\tau\mu} = 0.1$	4.146×10^{-3}	6.377×10^{-2}	9.866×10^{-2}	2.170×10^{-1}	3.813	1.115×10^{1}
Γ_H GeV $\rho_{\tau\mu} = 2.489 \times 10^{-2}$	4.176×10^{-3}	8.361×10^{-3}	2.477×10^{-2}	1.061×10^{-1}	3.665	1.097×10^{1}
σ_H (fb) $\rho_{\tau\mu} = 0.2$	5.428	6.380×10^{2}	4.428×10^{2}	2.337×10^{2}	4.078×10^{1}	8.919
σ_H (fb) $\rho_{\tau\mu} = 0.1$	7.790	6.040×10^{2}	3.766×10^{2}	1.541×10^{2}	1.149×10^{1}	2.353
σ_H (fb) $\rho_{\tau\mu} = 2.489 \times 10^{-2}$	7.725	2.883	9.389×10^{-1}	1.973×10^{-1}	7.483×10^{-3}	1.497×10^{-3}

Table 8: $\sqrt{s} = 8$ TeV Leptonic Decay with $\rho_{tc} = 2.501 \times 10^{-3}$

M_H	125 GeV	150 GeV	200 GeV	300 GeV	400 GeV	500 GeV
top Loop K-factor	1.89743	1.90633	1.92299	1.9447	1.91845	1.87137
bottom loop K-fator	1.04143	1.06498	1.10215	1.15453	1.19169	1.22052
Γ_H GeV $\rho_{\tau\mu} = 0.2$	5.950×10^{-3}	2.410×10^{-1}	3.350×10^{-1}	5.714×10^{-1}	4.286	1.174×10^{1}
Γ_H GeV $\rho_{\tau\mu} = 0.1$	4.146×10^{-3}	6.377×10^{-2}	9.866×10^{-2}	2.170×10^{-1}	3.813	1.115×10^{1}
Γ_H GeV $\rho_{\tau\mu} = 2.489 \times 10^{-2}$	4.176×10^{-3}	8.361×10^{-3}	2.477×10^{-2}	1.061×10^{-1}	3.665	1.097×10^{1}
σ_H (fb) $\rho_{\tau\mu} = 0.2$	1.173×10^{1}	1.426×10^{3}	1.053×10^{3}	6.200×10^{2}	1.196×10^{2}	8.919
σ_H (fb) $\rho_{\tau\mu} = 0.1$	1.566×10^{1}	1.350×10^{3}	8.956×10^{2}	4.088×10^{2}	3.370×10^{1}	7.580
σ_H (fb) $\rho_{\tau\mu} = 2.489 \times 10^{-2}$	1.669×10^{1}	6.446	2.233	5.232×10^{-1}	2.195×10^{-2}	4.822×10^{-3}

Table 9: $\sqrt{s} = 13$ TeV Leptonic Decay with $\rho_{tc} = 2.501 \times 10^{-3}$

M_H	125 GeV	150 GeV	200 GeV	300 GeV	400 GeV	500 GeV
top Loop K-factor	1.89743	1.90633	1.92299	1.9447	1.91845	1.87137
bottom loop K-fator	1.04143	1.06498	1.10215	1.15453	1.19169	1.22052
Γ_H GeV $\rho_{\tau\mu} = 0.2$	5.950×10^{-3}	2.410×10^{-1}	3.350×10^{-1}	5.714×10^{-1}	4.286	1.174×10^{1}
Γ_H GeV $\rho_{\tau\mu} = 0.1$	4.146×10^{-3}	6.377×10^{-2}	9.866×10^{-2}	2.170×10^{-1}	3.813	1.115×10^{1}
Γ_H GeV $\rho_{\tau\mu} = 2.489 \times 10^{-2}$	4.176×10^{-3}	8.361×10^{-3}	2.477×10^{-2}	1.061×10^{-1}	3.665	1.097×10^{1}
σ_H (fb) $\rho_{\tau\mu} = 0.2$	1.311×10^{1}	1.602×10^{3}	1.193×10^{3}	7.122×10^{2}	1.391×10^{2}	8.919
σ_H (fb) $\rho_{\tau\mu} = 0.1$	1.751×10^{1}	1.517×10^{3}	1.015×10^{3}	4.696×10^{2}	3.919×10^{1}	8.919
σ_H (fb) $\rho_{\tau\mu} = 2.489 \times 10^{-2}$	1.867×10^{1}	7.242	2.530	6.010×10^{-1}	2.552×10^{-2}	5.674×10^{-3}

Table 10: $\sqrt{s} = 14$ TeV Leptonic Decay with $\rho_{tc} = 2.501 \times 10^{-3}$

M_H	125 GeV	150 GeV	200 GeV	300 GeV	400 GeV	500 GeV
top Loop K-factor	1.89743	1.90633	1.92299	1.9447	1.91845	1.87137
bottom loop K-fator	1.04143	1.06498	1.10215	1.15453	1.19169	1.22052
Γ_H GeV $\rho_{\tau\mu} = 0.2$	5.950×10^{-3}	2.410×10^{-1}	3.350×10^{-1}	5.714×10^{-1}	4.286	1.174×10^{1}
Γ_H GeV $\rho_{\tau\mu} = 0.1$	4.146×10^{-3}	6.377×10^{-2}	9.866×10^{-2}	2.170×10^{-1}	3.813	1.115×10^{1}
Γ_H GeV $\rho_{\tau\mu} = 2.489 \times 10^{-2}$	4.176×10^{-3}	8.361×10^{-3}	2.477×10^{-2}	1.061×10^{-1}	3.665	1.097×10^{1}
σ_H (fb) $\rho_{\tau\mu} = 0.2$	9.600×10^{2}	1.828×10^{3}	1.340×10^{3}	7.390×10^{2}	1.278×10^{2}	8.958×10^{1}
σ_H (fb) $\rho_{\tau\mu} = 0.1$	3.204×10^{2}	1.731×10^{3}	1.139×10^{3}	4.872×10^{2}	3.601×10^{1}	7.134
σ_H (fb) $\rho_{\tau\mu} = 2.489 \times 10^{-2}$	2.145×10^{1}	8.262	2.841	6.237×10^{-1}	2.345×10^{-2}	4.538×10^{-3}

Table 11: $\sqrt{s} = 8$ TeV Hadronic Decay with $\rho_{tc} = 1.759 \times 10^{-3}$

M_H	125 GeV	150 GeV	200 GeV	300 GeV	400 GeV	500 GeV
top Loop K-factor	1.89743	1.90633	1.92299	1.9447	1.91845	1.87137
bottom loop K-fator	1.04143	1.06498	1.10215	1.15453	1.19169	1.22052
Γ_H GeV $\rho_{\tau\mu} = 0.2$	5.950×10^{-3}	2.410×10^{-1}	3.350×10^{-1}	5.714×10^{-1}	4.286	1.174×10^{1}
Γ_H GeV $\rho_{\tau\mu} = 0.1$	4.146×10^{-3}	6.377×10^{-2}	9.866×10^{-2}	2.170×10^{-1}	3.813	1.115×10^{1}
Γ_H GeV $\rho_{\tau\mu} = 2.489 \times 10^{-2}$	4.176×10^{-3}	8.361×10^{-3}	2.477×10^{-2}	1.061×10^{-1}	3.665	1.097×10^{1}
σ_H (fb) $\rho_{\tau\mu} = 0.2$	3.209×10^{1}	4.070×10^{3}	3.147×10^{3}	1.915×10^{3}	3.737×10^{2}	8.958×10^{1}
σ_H (fb) $\rho_{\tau\mu} = 0.1$	4.284×10^{1}	3.852×10^{3}	2.677×10^{3}	1.263×10^{3}	1.053×10^{2}	2.363×10^{1}
σ_H (fb) $\rho_{\tau\mu} = 2.489 \times 10^{-2}$	4.565×10^{1}	1.839×10^{1}	6.673	1.616	6.857×10^{-2}	4.822×10^{-3}

Table 12: $\sqrt{s} = 13$ TeV Hadronic Decay with $\rho_{tc} = 2.501 \times 10^{-3}$

M_H	125 GeV	150 GeV	200 GeV	300 GeV	400 GeV	500 GeV
top Loop K-factor	1.89743	1.90633	1.92299	1.9447	1.91845	1.87137
bottom loop K-fator	1.04143	1.06498	1.10215	1.15453	1.19169	1.22052
Γ_H GeV $\rho_{\tau\mu} = 0.2$	5.950×10^{-3}	2.410×10^{-1}	3.350×10^{-1}	5.714×10^{-1}	4.286	1.174×10^{1}
Γ_H GeV $\rho_{\tau\mu} = 0.1$	4.146×10^{-3}	6.377×10^{-2}	9.866×10^{-2}	2.170×10^{-1}	3.813	1.115×10^{1}
Γ_H GeV $\rho_{\tau\mu} = 2.489 \times 10^{-2}$	4.176×10^{-3}	8.361×10^{-3}	2.477×10^{-2}	1.061×10^{-1}	3.665	1.097×10^{1}
σ_H (fb) $\rho_{\tau\mu} = 0.2$	3.588×10^{1}	4.573×10^{3}	3.565×10^{3}	2.200×10^{3}	4.347×10^{2}	1.054×10^{2}
σ_H (fb) $\rho_{\tau\mu} = 0.1$	4.790×10^{1}	4.329×10^{3}	3.032×10^{3}	1.450×10^{3}	1.225×10^{1}	2.780×10^{1}
σ_H (fb) $\rho_{\tau\mu} = 2.489 \times 10^{-2}$	5.105×10^{1}	2.067×10^{1}	7.560	1.857×10^{-1}	7.976×10^{-2}	1.769×10^{-2}

Table 13: $\sqrt{s} = 14$ TeV Hadronic Decay with $\rho_{tc} = 2.501 \times 10^{-3}$